https://doi.org/10.5194/egusphere-2025-5656
Preprint. Discussion started: 18 December 2025

Global distribution of tetrafluoromethane (CF_4) and hexafluoroethane (C_2F_6) emissions determined by inverse modeling

Benjamin Püschel[1], Martin Vojta[1,2], Luise Kandler[1], Molly Crotwell[3,4], Andreas Engel[5], Paul B. Krummel[6], Chris R. Lunder[7], Jens Mühle[8], Simon O'Doherty[9], Ronald G. Prinn[10], Kieran M. Stanley[9], Isaac Vimont[4], Martin K. Vollmer[11], Thomas Wagenhäuser[5], Ray F. Weiss[8], Dickon Young[9], and Andreas Stohl[1]

[1]Department of Meteorology and Geophysics, University of Vienna, Vienna, Austria
[2]Department of Chemistry, University of Crete, Crete, Greece
[3]Cooperative Institute for Research in Environmental Sciences, University of Colorado, Boulder, Colorado, USA
[4]Global Monitoring Laboratory, National Oceanic and Atmospheric Administration, Boulder, Colorado, USA
[5]Institute for Atmospheric and Environmental Sciences, Goethe University of Frankfurt, Frankfurt, Germany
[6]CSIRO Environment, Aspendale, Victoria, Australia
[7]NILU, Kjeller, Norway
[8]Scripps Institution of Oceanography, University of California San Diego, La Jolla, California, USA
[9]School of Chemistry, University of Bristol, Bristol, UK
[10]Center for Sustainability Science and Strategy, Massachusetts Institute of Technology, Cambridge, Massachusetts, USA
[11]Laboratory for Air Pollution / Environmental Technology, Empa, Swiss Federal Laboratories for Materials Science and Technology, Dübendorf, Switzerland

Correspondence: Andreas Stohl (andreas.stohl@univie.ac.at)

Abstract.

The perfluorocarbons CF_4 and C_2F_6 are among the most potent greenhouse gases with lifetimes of fifty and ten thousand years, respectively. They are both primarily emitted during aluminum smelting and electronics manufacturing. We perform the first regionally resolved global inversion of CF_4 and C_2F_6, providing atmospheric measurement-based top-down emission estimates for 2006 – 2023 using the FLEXPART transport model and the FLEXINVERT+ framework.

Introducing a global-total constraint to align the inversion results with the relatively accurate global total emissions from the AGAGE 12-box model stabilizes the emissions in poorly monitored regions. Compared to the global bottom-up inventory EDGAR, the inversion increases global CF_4 and C_2F_6 emissions by factors of 2.6 ± 0.3 and 3.1 ± 0.7, respectively, for 2018 – 2023. China dominates global emissions, contributing 56% (CF_4) and 58% (C_2F_6) in 2018 – 2023. The contribution of South and Southeast Asia to global emissions rose from about 6% and 10% in 2006 – 2011 to 22% and 18% by 2018 – 2023, respectively, though large uncertainties remain due to a lack of measurements in the region itself. European emissions declined until 2010, then stabilized and contribute 2% – 3% to global emissions by 2018 – 2023. U.S. CF_4 emissions remain constant and C_2F_6 emissions decreased steadily (reaching 3% – 4% by 2018 – 2023), with a temporary drop in 2009 likely linked to the financial crisis. On the global scale, our results suggest a contribution of 81% by the aluminum industry to total CF_4 emissions and 48% by the electronics industry to total C_2F_6 emissions.

https://doi.org/10.5194/egusphere-2025-5656
Preprint. Discussion started: 18 December 2025

1 Introduction

The perfluorocarbons (PFCs) tetrafluoromethane (CF_4, PFC-14) and hexafluoroethane (C_2F_6, PFC-116) are two of the most potent greenhouse gases (GHGs) with global warming potentials (GWPs) of approximately 7,490 and 12,600 over a 100-year period (Hodnebrog et al., 2020). Due to their high inertness against removal processes in the atmosphere, the unintended removal during high-temperature combustion is assumed to be their major sink (Cicerone, 1979; Ravishankara et al., 1993). Lifetime estimates are around 50,000 and 10,000 years (IPCC, 2023), respectively, and therefore CF_4 and C_2F_6 alter the global radiative balance essentially permanently on human time scales. Unlike most fluorinated greenhouse gases (F-gases), CF_4 has a known natural source, i.e., its release from calcium fluorite in the continental crust, which produced a stable pre-industrial background mole fraction of 34.1 ± 0.3 ppt (Trudinger et al., 2016). In contrast, the natural background of C_2F_6 is estimated to be zero or negligibly small (Trudinger et al., 2016). Anthropogenic activity has led to the global increase in CF_4 and C_2F_6 mole fractions to currently about 90 ppt and 5 ppt, respectively. The resulting contribution to Earth's radiative imbalance is approximately 0.2% compared to all well-mixed GHGs in 2019 with respect to 1750 (IPCC, 2023). While currently this value is arguably relatively small, the PFC contribution will increase considerably if emissions of shorter-lived GHGs cease in the future, especially if anthropogenic PFC emissions continue.

CF_4 and C_2F_6 are emitted from the electrolysis process used by the primary aluminum industry during irregular events, referred to as anode effects. These events reflect a temporary imbalance in the electrochemical smelting process, typically due to poor mixing or low alumina concentration in the reduction cell. This leads to a sharp increase in cell voltage and causes PFCs to form which can be released into the atmosphere (Tabereaux and Peterson, 2014; Marks and Bayliss, 2011). Wong et al. (2015) also suspect PFC formation and emission during standard smelting conditions and low-voltage anode effects leading to higher emissions than previously assumed. The second major source of emissions is the electronics industry, where PFCs are used as etchants and cleaning agents to produce semiconductors, flat panel displays and photovoltaic cells. Despite the implementation of end-of-pipe abatement systems, significant fractions of the utilized CF_4 and C_2F_6 are still released into the atmosphere (Illuzzi and Thewissen, 2010; Calvo Buendia et al., 2019). Other PFC sources include the smelting of rare earth metals, use as refrigerants, and fugitive emissions during the chemical production of the gases themselves. Some of these processes could contribute substantially to global emissions, but current estimates are highly uncertain (Kim et al., 2014; Cai et al., 2018; Vogel and Friedrich, 2018). The fractional attribution of global emissions to each contributing sector varies significantly in different emission inventories. Generally, the aluminum and electronics industries are estimated to account for around 60 – 80% and 20 – 40% of global emissions, respectively, while miscellaneous emissions likely represent less than 5% for both species (EDGAR, 2024; Kim et al., 2021). Emissions from the global aluminum industry are CF_4-dominated, with a C_2F_6/CF_4 ratio of approximately 0.1 kg kg^{-1}, while the electronics sector emits a larger share of C_2F_6, with a ratio around 0.4 kg kg^{-1} (Kim et al., 2014).

Alongside regulations of CF_4 and C_2F_6 emissions under the Kyoto Protocol (UNFCCC, 1997) and the Paris Agreement (UNFCCC, 2015), the aluminum and electronics industries themselves have undertaken efforts to reduce their PFC emissions (e.g. Marks and Bayliss, 2011; IAI, 2020; WSC, 2011, 2024). Emission reporting is carried out both voluntarily by industries

https://doi.org/10.5194/egusphere-2025-5656
Preprint. Discussion started: 18 December 2025

and formally by individual countries through official submissions to the United Nations Framework Convention on Climate Change (UNFCCC). However, only countries listed under Annex I are required to report emissions annually to the UNFCCC, while most other countries publish emissions at different irregular intervals (UNFCCC, 1997, 2024a, b). Various bottom-up (BU) estimates (i.e. using industry consumption or activity data to infer emissions) are compiled in a global inventory by the Emissions Database for Global Atmospheric Research F-GASES version 2024 (EDGAR, 2024).

After a period of decreasing emissions between approximately 1990 (2000 for C_2F_6) and 2010, emissions were found to increase again over the past 15 years, according to global measurement based top-down (TD) emission estimates using the AGAGE 12-box model (Mühle et al., 2010; Rigby et al., 2014; Trudinger et al., 2016; Say et al., 2021; Western et al., 2025b). Performing regional inverse modeling of PFC emissions from East Asia and China, Arnold et al. (2018), Kim et al. (2021), An et al. (2024) and Chen et al. (2025) found that China has been the largest PFC emitter in recent years, accounting for approximately $42–66\%$ and $38–64\%$ of global CF_4 and C_2F_6 emissions, respectively.

In addition, there are large gaps between BU and TD emission estimates. BU-based emission inventories report global values as low as half of those from TD methods in recent years and often fail to capture the recent upward trend (Kim et al., 2021; EDGAR, 2024; UNFCCC, 2024a, b). For Northwest Europe, Say et al. (2021) found significantly higher emissions in their regional inverse modeling results compared to the countries' own estimates, reported to the UNFCCC. However, this discrepancy contributes little to the global TD – BU gap, as the region's share of the global total PFC emissions is relatively small. Similarly, for Australia, Dunse et al. (2019) reported higher emissions applying TD inverse modeling methods compared to the Australian BU inventory submitted to the UNFCCC, also with minimal impact on the global discrepancy. Kim et al. (2021) suggested that 25% (CF_4) and 77% (C_2F_6) of the global TD – BU discrepancy can be attributed to East Asian countries during 2012 to 2018. These results suggest that previously investigated regions, particularly China and East Asia, are not the only contributors to the global TD – BU discrepancy. There is need for more TD emission estimates in regions such as South and Southeast Asia, North America, South America and Africa to close this gap and identify other contributing regions (Kim et al., 2021; Guo and Fang, 2024).

Therefore, we present the first regionally resolved, global TD emission estimates for the period 2006 to 2023 using inverse modeling and data from global networks measuring atmospheric CF_4 and C_2F_6 mole fractions. To overcome the difficulty of weak observational constraints in poorly observed regions, we introduce a novel method to constrain the total global emission result of the regionally resolved model to the more robust global emission results from the AGAGE 12-box model simulations. We compare our results to existing regional and global BU and TD emission estimates from various previous studies and reports (Mühle et al., 2010; Trudinger et al., 2016; Arnold et al., 2018; Western et al., 2025b; Kim et al., 2021; Guo et al., 2023; An et al., 2024; EDGAR, 2024; UNFCCC, 2024a, b). Finally, we use the C_2F_6/CF_4 emission ratios to infer relative contributions from the aluminum and electronics industries.

https://doi.org/10.5194/egusphere-2025-5656
Preprint. Discussion started: 18 December 2025

2 Methods

2.1 Measurement data

The inversion is constrained by continuous in situ and flask sample atmospheric mole fraction measurements from 52 observation stations worldwide (Fig. 1), operated by various networks and institutions. Information on the measurement sites, including their location, affiliation, measurement intervals and periods with available data are provided in Tables S1-S3.

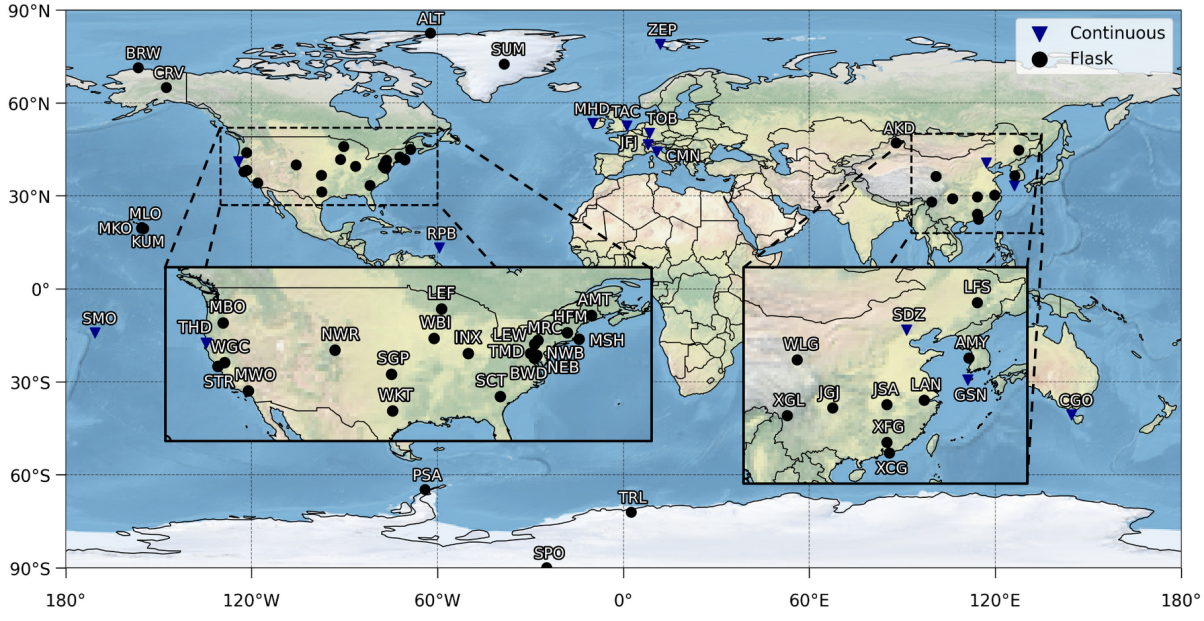

Figure 1. Map of measurement stations used in the inversion. Continuous monitoring sites are marked with black triangles, flask sampling sites with black dots. Sites in the United States and in eastern China are shown also in zoomed insets. Three-letter codes refer to the list of stations shown in Table S1.

The Advanced Global Atmospheric Gases Experiment (AGAGE) (Prinn et al., 2025, 2018) network CF_4 and C_2F_6 measurements started in the mid 2000s, expanding to the 11 sites used here, using "Medusa" pre-concentration gas chromatography and mass spectrometry (GC-MS) systems at intervals of approximately every 2 hours (Miller et al., 2008). A network of stainless steel and glass flask measurements from 29 individual surface stations, primarily located in North America is operated by the National Oceanic and Atmospheric Administration, Earth System Research Laboratories, Global Monitoring Laboratory (NOAA-ESRL-GML) Long-term Observations of Greenhouse gases and Ozone-depleting Substances (LOGOS) division (Vimont et al., 2025) providing measurements at daily to monthly resolution since 2015. NOAA-ESRL-GML flask samples are measured using the PERSEUS-1 GC-MS instrument. C_2F_6 measurements are only available for a subset of 10 stations, while CF_4 mole fractions are reported for all stations. Atmospheric mole fraction measurements at one continuous (2 h resolution) and eight flask sampling stations (1 day or 1 week resolution) in China, performed by the China Meteorological Administration

https://doi.org/10.5194/egusphere-2025-5656
Preprint. Discussion started: 18 December 2025

(CMA), have recently been published by An et al. (2024) for the period 2011 to 2021. Medusa GC-MS systems were used for both continuous and flask measurements. Additionally, daily measurements using the ODS5-pro GC-MS system at the Xichong station in China, provided by Chen (2025), are used for the inversion. At the Trollhaugen station in Antarctica, operated by NILU, steel flask samples are collected and measured using the Medusa GC-MS system at NILU (Lunder, 2024). No conversion is needed between the SIO-05/SIO-07 (AGAGE, CMA, Xichong, Trollhaugen) and SIO-05-b/SIO-07-b (NOAA-ESRL-GML) calibration scales for CF_4 and C_2F_6, since relative differences are smaller than 0.1% and 1%, respectively.

Overall measurement precisions are estimated to be better than 1% for both species except for C_2F_6 measurements at Xichong, where they are 5%. Continuous in situ measurements performed by AGAGE have precisions of typically 0.15% or better for CF_4 and 0.7% or better for C_2F_6. However, the instrument precisions are not used in the inversion as they are much lower than the total assumed observation uncertainty, which includes model and representation errors (see Sect. 2.2). To reduce the influence of model correlations between samples, we averaged all observational data over 3 h intervals, resulting in an average of 12,413 and 13,048 measurement samples per year used in the inversion for CF_4 and C_2F_6, respectively.

Figure 2 presents the number of measurement samples in East Asia, Europe, North America, the Southern Hemisphere, and all other regions, along with the total number of measurement sites per year for CF_4 and C_2F_6. While some stations in the AGAGE network began measuring as early as 2003, observations remained too sparse before 2006 to expect significant improvements in regionally resolved emission estimates. Particularly the AGAGE station in Gosan (South Korea) contributes to a higher constraint on emissions when it started to operate in 2007, enabling relatively robust results in our regionally resolved global inversion. The number of stations and observations generally rises until 2021 but decreases during the last two years mainly due to the unavailability of CMA observations from East Asia.

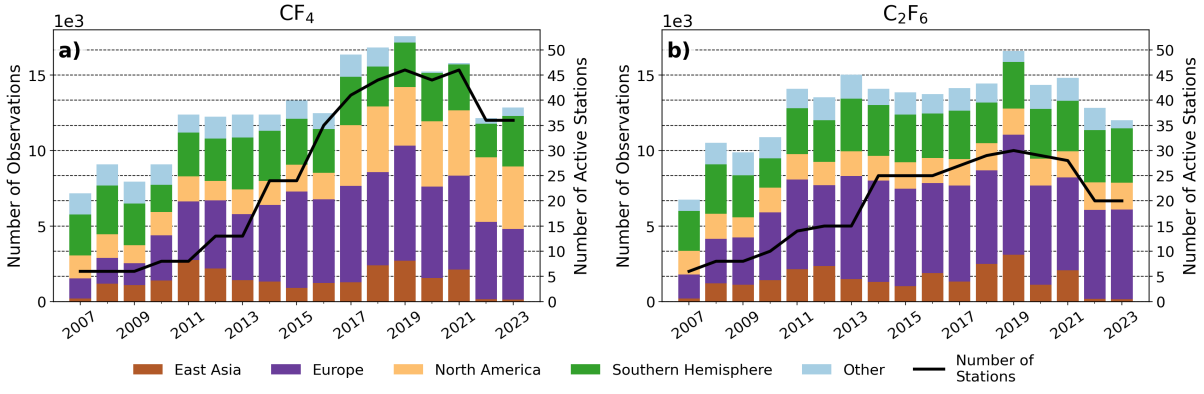

Figure 2. Number of individual observations used in the inversion by region (see label bar for regional color coding) as well as number of operating stations (black line) for the years 2007 to 2023 for CF_4 (a) and C_2F_6 (b), respectively.

https://doi.org/10.5194/egusphere-2025-5656
Preprint. Discussion started: 18 December 2025

2.2 Inversion method

To estimate how sensitive the measurements at each station are to regionally resolved emissions, we simulate atmospheric transport explicitly using the Lagrangian particle dispersion model (LPDM) FLEXPART 10.4 (Stohl et al., 1998; Pisso et al., 2019). For each station and time of each averaged measurement sample, 50,000 chemically inert particles are released and tracked backwards in time for 100 days. The particularly long backward simulation period is motivated by the findings of Vojta et al. (2022), who showed that a longer period (50 d) can lead to more robust inversion results compared to shorter periods (1 – 20 d). With a sparse measurement network, a long backward simulation period can increase the observational constraint in remote regions with a large distance to measurement stations. While this does not provide a highly resolved constraint in these regions, it improves the consistency of the regionally resolved inversion results with the relatively well known global emissions (Vojta et al., 2022). Hourly ECMWF (European Centre for Medium-Range Weather Forecasts) ERA5 reanalysis data (Hersbach et al., 2020) with a horizontal resolution of $0.5° \times 0.5°$ and 137 vertical levels serve as input for FLEXPART. Since emissions are assumed to occur mostly near the surface, particle positions in the lowest 100 m of the atmosphere are used to obtain the emission sensitivities on a $1° \times 1°$ grid at daily intervals. Particle positions at the trajectory end (i.e. after 100 d of backward tracking) are saved on the same horizontal grid, on 12 vertical levels with upper boundaries at 0.1, 0.5, 1, 2, 3, 5, 7, 9, 12, 15, 20, 50 km, respectively, and represent the sensitivity to initial mole fractions or termination sensitivity. The sensitivity of observation stations to emissions is shown in figure 3 as an average over model simulations from all observation stations in the year of 2019. Emission sensitivities are naturally highest close to measurement stations as well as in the prevailing wind direction from each station. As can be seen, emission sensitivities are still low in certain regions (e.g., South America, Africa, the Maritime Continent or India), despite the long backward tracking time.

Since CF_4 and C_2F_6 are long-lived species, emissions occurring prior to the backward simulation period also influence measured mole fractions and need to be accounted for by introducing a baseline of mole fractions. The baseline is constructed using the global-distribution-based (GDB) method where the sensitivity to initial conditions at the particle termination points is coupled to custom global three-dimensional reanalyses of CF_4 and C_2F_6 mole fractions (Vojta et al., 2022). Since no such reanalysis is available, the linear chemistry module (LCM) of FLEXPART 11 (Bakels et al., 2024) is used to explicitly model the emission and transport of CF_4 and C_2F_6 between 2005 and 2023. Assimilating observed mole fractions into FLEXPART-LCM keeps the model results close to the observations. Daily mole fraction fields representing the reanalysis are stored and coupled to the termination sensitivity output of the FLEXPART backward simulations. Further information on the reanalysis simulation can be found in Supplement S2.

In the inversion, a pure optimization of emissions to produce the best fit of model results to observations would result in a mathematically under-determined problem and lead to overfitting, especially in regions where the observational constraint is weak. To stabilize the solution of the inversion, an additional constraint on the desired emissions is required. For that, a priori emissions based on the Emissions Database for Global Atmospheric Research F-GASES version 2024 (EDGAR, 2024) are used, providing global gridded emissions at $0.1° \times 0.1°$, downscaled to $1° \times 1°$ resolution. After preliminary review of the EDGAR dataset, we decided to adjust unrealistically low emissions of CF_4 and C_2F_6 in China, India and South Korea.

https://doi.org/10.5194/egusphere-2025-5656
Preprint. Discussion started: 18 December 2025

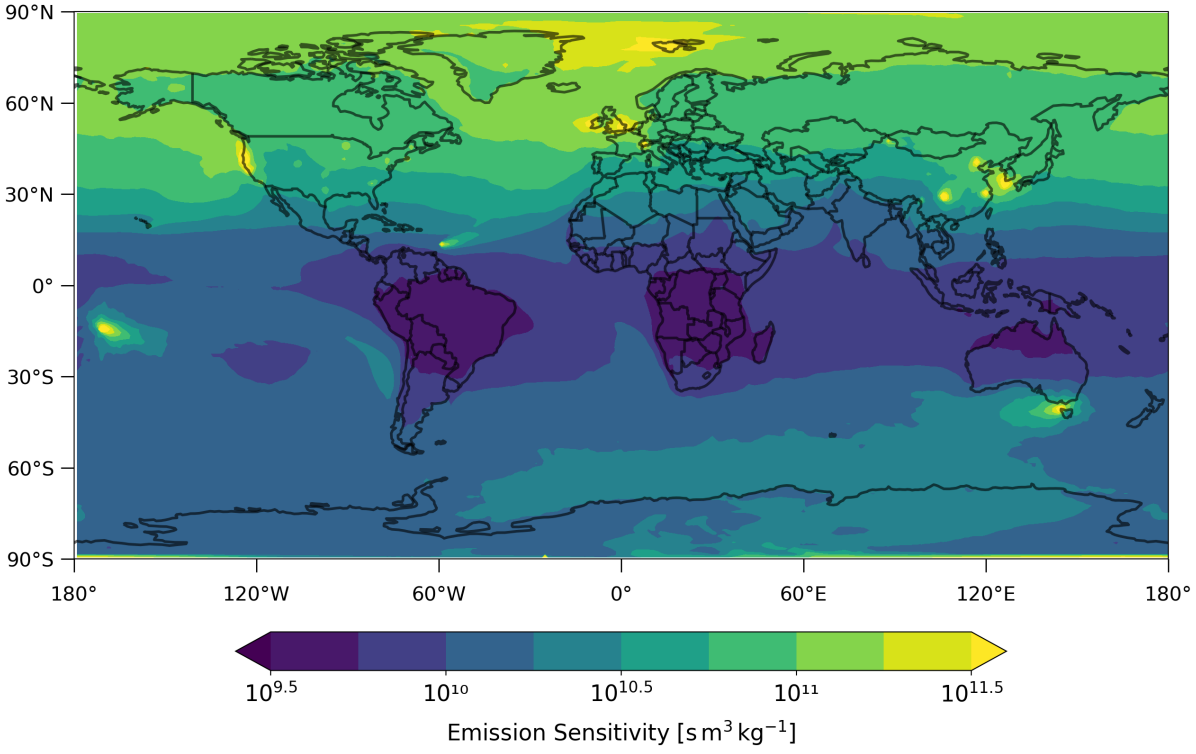

Figure 3. Temporally averaged emission sensitivity of all available CF_4 measurements in the year 2019. All transport simulations initiated from their corresponding 3 h observation averaging interval were weighted equally, regardless of the observation frequency and type. Consequently, emission sensitivities are higher near stations with higher measurement frequency than near stations with lower frequency.

The emission spatial distribution of EDGAR is kept in all cases, but the magnitude is adjusted using BU-based data by Guo et al. (2023) in China, the reported value to the UNFCCC for 2020 (MoEFCC, 2024), extrapolated using primary aluminum production data (British Geological Survey, 2025) in India, and reported emissions to the UNFCCC (UNFCCC, 2024a) in South Korea. The adjustment significantly increases global emission by 31% for CF_4 and 38% for C_2F_6 on average compared to EDGAR and brings them closer to the well known global total emissions from TD studies (Western et al., 2025b), yet still underestimates them.

Emissions are estimated annually on a variable resolution $8° \times 8°$ to $1° \times 1°$ grid where ocean cells are excluded, leading to 7,789 individual grid cells per year to increase computational efficiency compared to a global $1° \times 1°$ grid (see Fig. S1). The inversion is performed using the Bayesian inversion framework FLEXINVERT+ (Thompson and Stohl, 2014) which estimates the a posteriori emission state vector $\boldsymbol{x}$ by minimizing the difference between measured ($\boldsymbol{y}$) and modeled ($\mathbf{H}\boldsymbol{x}$) mole fractions while simultaneously being constrained by the a priori emissions $\boldsymbol{x}_p$. $\mathbf{H}$ represents the atmospheric transport operator containing the emission sensitivities that relate gridded emissions to individual measurement locations and sample times. With Gaussian-distributed uncertainties, the cost function that yields the optimal a posteriori emissions when minimized is:

https://doi.org/10.5194/egusphere-2025-5656
Preprint. Discussion started: 18 December 2025

$$J(\boldsymbol{x}) = \frac{1}{2}(\boldsymbol{x} - \boldsymbol{x}_p)^T \mathbf{B}^{-1}(\boldsymbol{x} - \boldsymbol{x}_p) + \frac{1}{2}(\mathbf{H}\boldsymbol{x} - \boldsymbol{y})^T \mathbf{R}^{-1}(\mathbf{H}\boldsymbol{x} - \boldsymbol{y}), \tag{1}$$

where $\mathbf{B}$ is the a priori emission error covariance matrix and $\mathbf{R}$ represents the observation error covariance matrix (see Thompson and Stohl (2014) for a more detailed explanation of the error covariance matrices, state, and observation vectors). The magnitudes of $\mathbf{B}$ and $\mathbf{R}$ balance the influence of a priori emissions and measurements. $\mathbf{B}$ is constructed by assuming an uncertainty of 500% per grid cell with a minimal uncertainty of $1 \times 10^{-13}\,\mathrm{kg\,h^{-1}\,m^{-2}}$ and $2 \times 10^{-14}\,\mathrm{kg\,h^{-1}\,m^{-2}}$ for CF_4 and C_2F_6, respectively, and spatial correlation using an exponential decay with scale length of $100\,\mathrm{km}$. The baseline is also optimized during the inversion and is given an uncertainty of $0.5\,\mathrm{ppt}$ and $0.1\,\mathrm{ppt}$ for CF_4 and C_2F_6, respectively, as estimated during a test reanalysis simulation where a subset of measurements was used for validation only. The observation error covariance matrix $\mathbf{R}$ accounts for uncertainty of the measurements, the model transport and representation error, however ignores potential correlations between observations and model representations and is therefore assumed to be diagonal. To address errors of the model and its representation of the measurements, a simplified approach adapted from Henne et al. (2016) or Bergamaschi et al. (2022) is adopted here, where an arbitrary uncertainty of $2.0\,\mathrm{ppt}$ and $0.4\,\mathrm{ppt}$ is assigned to measurements below $120\,\mathrm{ppt}$ and $6\,\mathrm{ppt}$ for CF_4 and C_2F_6, respectively. For measured mole fractions above these thresholds the assigned uncertainty increases linearly to account for poorer representation of atmospheric transport to measurements strongly influenced by close-by emissions. Finally, minimizing the cost function (Eq. 1) yields the following analytical solution for the a posteriori emission state (e.g. Tarantola, 2005):

$$\boldsymbol{x} = \boldsymbol{x}_p + (\mathbf{B}^{-1} + \mathbf{H}^T\mathbf{R}^{-1}\mathbf{H})^{-1}\mathbf{H}^T\mathbf{R}^{-1}(\boldsymbol{y} - \mathbf{H}\boldsymbol{x}_p), \tag{2}$$

while the a posteriori emission error covariance matrix $\mathbf{A}$ is expressed as:

$$\mathbf{A} = \mathbf{B} - (\mathbf{B}^{-1} + \mathbf{H}^T\mathbf{R}^{-1}\mathbf{H})^{-1}\mathbf{H}^T\mathbf{R}^{-1}\mathbf{H}\mathbf{B}. \tag{3}$$

FLEXINVERT+ outputs the a posteriori emissions and uncertainties on both a regular $1^\circ \times 1^\circ$ grid as well as on the variable grid for further analysis and post-processing (see Sect. 2.3). Additionally, modeled a posteriori-, a priori-, a posteriori baseline- and a priori baseline mole fractions are written by FLEXINVERT+. The modeled mole fractions together with measured mole fractions for the three exemplary stations Tacolneston (England), Trinidad Head (U.S.), and Jiangjin (China) are presented in figure S2-S4. More detail on the inversion framework FLEXINVERT+ is provided by Thompson and Stohl (2014).

For analysis of national and regional emission estimates, emissions were masked according to political borders. Given the $1^\circ \times 1^\circ$ resolution, emissions in grid cells overlapping multiple regions' territories are apportioned based on the fractional land area of each region within the respective grid cell. A priori and a posteriori uncertainties for each region follow the approach of Henne et al. (2016), applying a mask vector to the respective error covariance matrix and accounting for correlations between grid cells. To correctly quantify the uncertainty associated with regions containing multiple grid cells, Gaussian error propagation was applied.

https://doi.org/10.5194/egusphere-2025-5656
Preprint. Discussion started: 18 December 2025

2.3 Constraint to global emission sum

Global inversions of CF_4 and C_2F_6 emissions based on explicitly modeled atmospheric transport suffer from a sparse measurement network, resulting in weak constraints in some regions, particularly over tropical and Southern Hemisphere land areas. Issues arising from this limitation include spurious adjustment of emissions or no adjustment of biased prior emissions in weakly constrained regions, which can lead to global total emissions that deviate significantly from well-known global emissions. To address these issues, we introduce a novel approach to constrain the sum of the global emission estimate from FLEXINVERT+ to less uncertain total global estimates from a simpler, low-resolution inversion model. Here, we take estimates from AGAGE 12-box model simulations by Western et al. (2025b) (Dataset: Western et al., 2025a), which are reliable in their total global estimate, but lack regional resolution. The approach is implemented as a post processing step, requiring the a posteriori emission state vector $\boldsymbol{x}$ and a posteriori emission error covariance matrix $\mathbf{A}$ as input to obtain the constrained a posteriori emissions $\boldsymbol{x}_c$ with the following equation:

$$\boldsymbol{x}_c = \boldsymbol{x} + \mathbf{A}\mathbf{P}^T(\mathbf{P}\mathbf{A}\mathbf{P}^T + \mathbf{C})^{-1}(\boldsymbol{c} - \mathbf{P}\boldsymbol{x}). \tag{4}$$

Here, $\boldsymbol{c}$ represents a vector containing annual global emission estimates from the AGAGE 12-box model, while the matrix $\mathbf{C}$ contains uncertainties of the emission values on its diagonal. $\mathbf{P}$ is a matrix of ones yielding a vector of annual sums of emissions from FLEXINVERT+ when applied to $\boldsymbol{x}$. The deviation of the total global FLEXINVERT+ values from the AGAGE 12-box model results is regionally distributed according to the a posteriori error covariance matrix $\mathbf{A}$, leading to a higher attribution of the deviation to grid cells with higher uncertainty and vice versa. The constraint method predominantly affects regions with low observational constraint and simultaneously high emissions (i.e. high emission uncertainty) while exerting minimal influence on the emissions in well-observed regions. Its implementation follows the method to constrain negative emissions toward 0 using the truncated Gaussian approach by Thacker (2007), which was additionally applied to the constrained a posteriori emissions in this study.

2.4 Industry specific emission estimates

We apply an approach introduced by Kim et al. (2014) using C_2F_6/CF_4 emission ratios to determine the relative contributions of the aluminum and electronics sectors to total emissions. Using air mass trajectory analysis and in situ mole fraction measurements, Kim et al. (2014) calculated emission ratios when pollution plumes came from either aluminum smelting facilities or electronics industry locations. They estimated the emission ratios at $r_{al} = 0.10 \pm 0.01\,\mathrm{kg\,kg^{-1}}$ for the aluminum industry and $r_{el} = 0.40 \pm 0.19\,\mathrm{kg\,kg^{-1}}$ for the semiconductor industry which we assume can be extended to the whole electronics industry. It is important to note that these ratios were calculated in the late 2000s for Australian aluminum smelters and electronics industries in Japan, South Korea and Taiwan but are assumed here to be equal for industries across the globe and for recent years as well. Calculating emission ratios from several BU inventories (EDGAR, 2024; UNFCCC, 2024a, b; Guo et al., 2023), with either industry-specific data or emission data in countries where one sector is known to be significantly larger than the other,

https://doi.org/10.5194/egusphere-2025-5656
Preprint. Discussion started: 18 December 2025

emission ratios appear to be stable across regions and time, particularly for the aluminum industry ratio. The electronics industry ratio is more variable across countries, but this fact is taken into account with the significantly higher uncertainty of r_{el}. Finally, sector specific emissions can be estimated when emissions for CF_4 and C_2F_6 are known using a simple set of equations described by Kim et al. (2014) (Sect. 2.2). We apply this approach here to split our a posteriori emissions into contributions from the aluminum and electronics industries, respectively, and investigate their changes from the a priori contributions.

3 Results

In the following sections, we present our inversion results and compare them to other TD emission estimates as well as BU inventories. We average inversion results over three 6-year intervals (early: 2006 – 2011, mid: 2012 – 2017, late: 2018 – 2023), unless specified otherwise, to reduce the influence of model-related inter-annual variability in our analysis. The specified uncertainty ranges for the averaged inversion results combine the standard error derived from the variability of the data within each averaging interval and the analytical standard error derived by the inversion model, propagated using Gaussian error propagation. For all further analysis, the FLEXINVERT+ output, constrained to total global emission values from the AGAGE 12-box model, is used as our main inversion result. For comparison, we also show results obtained without this extra constraint in all time series plots.

3.1 Global emissions and emission share

Figure 4 shows the inversion-derived global total a posteriori emissions, both with and without global constraint, compared to the AGAGE 12-box model results by Western et al. (2025b) and the BU inventories by EDGAR (2024), UNFCCC (2024a, b), and our adjusted BU inventory used as a priori emission information. The global unconstrained FLEXINVERT+ results are already relatively close to the AGAGE 12-box model reference values, but exhibit high interannual variability, particularly in the earliest and latest years when observational coverage is lowest. The inversion performance, indicated by the global error reduction, varies between different years and is closely correlated with the number and spatial distribution of available measurements. The globally constrained results align closely with box-model emissions, as intended by this method.

Our global emissions amount to $10.8 \pm 2.0\,\mathrm{kt\,yr^{-1}}$ and $2.2 \pm 0.5\,\mathrm{kt\,yr^{-1}}$ in the early period (2006-2011), $12.2 \pm 1.6\,\mathrm{kt\,yr^{-1}}$ and $2.1 \pm 0.5\,\mathrm{kt\,yr^{-1}}$ in the mid period (2012-2017), and $15.3 \pm 1.6\,\mathrm{kt\,yr^{-1}}$ and $2.4 \pm 0.4\,\mathrm{kt\,yr^{-1}}$ in the late period (2018-2023) for CF_4 and C_2F_6, respectively. This corresponds to emission increases of $42 \pm 25\,\%$ and $12 \pm 33\,\%$ for the two species between the early and late period. CF_4 emissions experience a persistent growth over the whole study period, while emissions of C_2F_6 dropped in the late 2000s and increased again over the 2010s. For both species, the lowest emissions are observed after the global financial crisis in 2008, which led to reduced aluminum demand and production. Our results do not indicate an emission decrease during the COVID-19 pandemic beginning in 2020, consistent with aluminum industry reports indicating no significant production decrease (IAI, 2021). It is difficult to assess the impact of those crises on emissions of PFCs by the electronics industry, as these gases are used in various manufacturing steps and technologies. However, from the stronger

https://doi.org/10.5194/egusphere-2025-5656
Preprint. Discussion started: 18 December 2025

increase of CF_4 compared to C_2F_6 we can infer a global shift of PFC emissions toward the aluminum industry, assuming industry-specific emission ratios remained relatively constant.

Our inversion results are 2.6 ± 0.3 and 3.1 ± 0.7 times higher than the EDGAR BU inventory emissions in the most recent period, likely indicating that EDGAR underestimates the true emissions, which had also been concluded from earlier box model results (Say et al., 2021). Emissions reported to the UNFCCC are too low as well, and highly variable due to the irregular reporting by some major emitting countries, making the data difficult to compare on a global scale. Our custom BU inventory, compiled from EDGAR's dataset with adjustments in India, China, and South Korea using other BU sources, has higher emissions than the original EDGAR inventory and occasionally overlaps with our results within the uncertainty range, but also consistently underestimates the emissions.

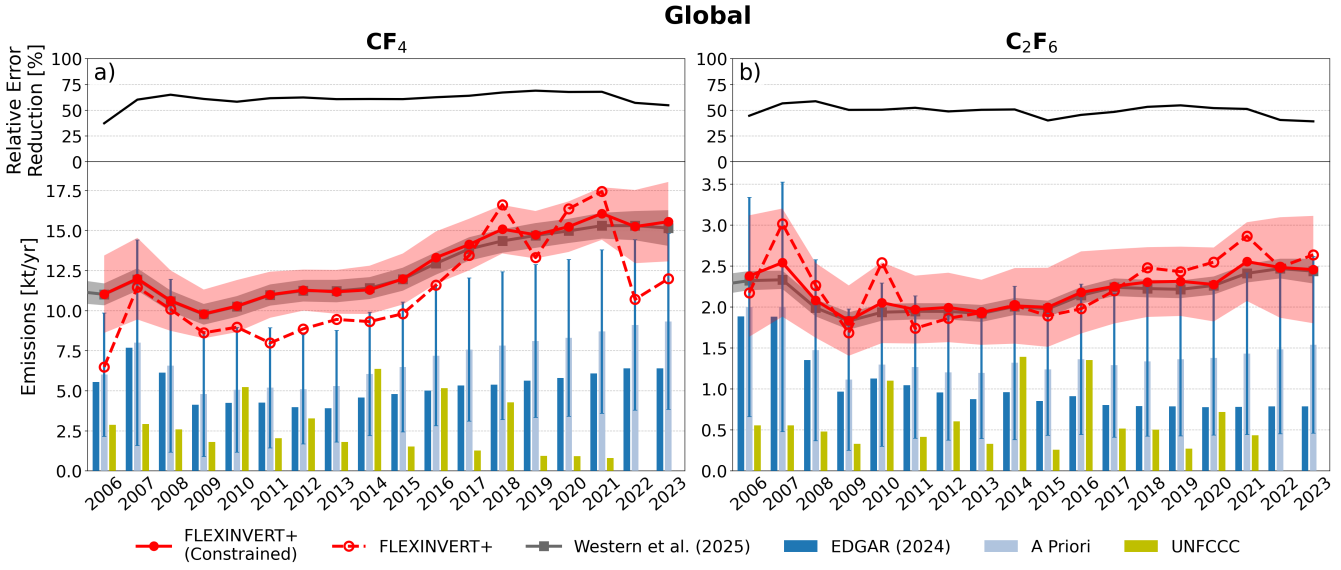

Figure 4. Global emissions of CF_4 (a) and C_2F_6 (b) for the period 2006 – 2023 from the original BU emission inventory EDGAR (2024) (dark blue bars), our adjusted BU a priori inventory (light blue bars, with assigned a priori uncertainty ranges given by whiskers), the UNFCCC (2024a, b) reports (light green bars), the AGAGE 12-box model results of Western et al. (2025b) (grey line with grey shading indicating uncertainty), our globally constrained inversion results (solid red line with shading indicating uncertainty), and our globally unconstrained inversion results (red dashed line). The relative error reduction by the inversion is shown in the upper panels.

Figure 5 gives an overview of the contribution of individual regions to global CF_4 and C_2F_6 emissions for our three six-year periods. The diagrams show each region's globally constrained inversion results as relative contributions to the global total. For CF_4, the largest emission shares are attributed to China at $50 \pm 20\%$, $63 \pm 14\%$, and $56 \pm 13\%$ in the three periods, rising from the early to the mid and then decreasing again toward the late period. China's large share is driven by the country's large aluminum industry, producing around 60% of global aluminum, as well as its electronics industry. In the early period, China is followed by Russia, the current 27 countries of the European Union (EU), and the U.S. with minor emission contributions by

https://doi.org/10.5194/egusphere-2025-5656
Preprint. Discussion started: 18 December 2025

South Korea, Japan, Taiwan, India and Malaysia+Singapore (Malaysia and Singapore are grouped due to Singapore's small size but significant emissions). Toward the mid and late period, India's emission share rises rapidly, while other regions' relative contributions decrease, particularly those of Russia, the EU, the U.S., and Japan. Only Malaysia+Singapore's contribution also increased, although these values are associated with large uncertainties, making the trend insignificant. This development coincides with the shift of the aluminum and electronics industries toward South, Southeast, and East Asia during this time and the implementation of more efficient aluminum smelting technology, exhaust abatement systems, and PFC replacement by electronics manufacturers in Europe and North America (Tan et al., 2025; Czerniak, 2018).

China is also the largest emitter of C_2F_6, exhibiting a rapidly rising emission contribution from $34 \pm 27\%$ in the early to $50 \pm 25\%$ in the middle and $58 \pm 23\%$ in the late period. Due to the higher C_2F_6/CF_4 emission ratio by the electronics industry, the emission trends indicate a shift of China's emissions from the aluminum to the electronics industry. Similar to CF_4, the C_2F_6 emission contribution decreased substantially in the EU, the U.S., as well as in Japan, South Korea, and Taiwan - regions where emissions are generally dominated by the electronics industry. Emissions in Russia and Malaysia+Singapore follow the global trend relatively closely, while India's emission share increases rapidly during this time period.

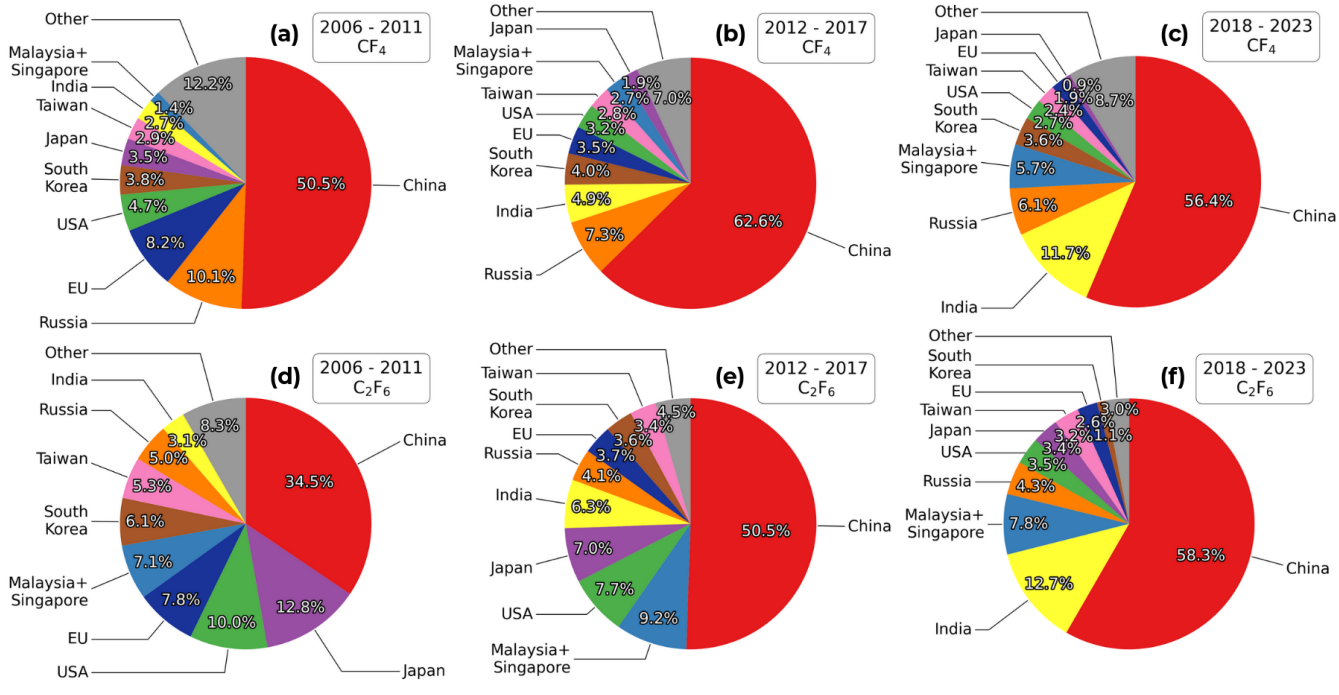

Figure 5. Relative contributions of individual countries to global total emissions of CF_4 (a – c) and C_2F_6 (d – f) for the periods 2006 – 2011 (a and d), 2012 – 2017 (b and e) and 2018 – 2023 (c and f) according to the globally constrained inversion results.

https://doi.org/10.5194/egusphere-2025-5656
Preprint. Discussion started: 18 December 2025

3.2 Regional emissions

As the largest PFC emitter, China is the strongest driver of global trends of CF_4 and C_2F_6 emissions in recent years. Figure 6 presents a time series of China's emissions, comparing our inversion results to other TD and BU estimates. According to our globally constrained inversions, CF_4 and C_2F_6 emissions rose steadily from $4.6 \pm 1.0\,\mathrm{kt\,yr^{-1}}$ and $0.70 \pm 0.24\,\mathrm{kt\,yr^{-1}}$ in the early period to $6.6 \pm 0.7\,\mathrm{kt\,yr^{-1}}$ and $0.98 \pm 0.16\,\mathrm{kt\,yr^{-1}}$ in the mid period and to $8.3 \pm 0.8\,\mathrm{kt\,yr^{-1}}$ and $1.46 \pm 0.19\,\mathrm{kt\,yr^{-1}}$ in the late period. However, we note that results for China in the years 2006, 2007, 2022, and 2023 are associated with high uncertainty due to the low number of observations, leading to less error reduction in these years.

China's CF_4 emissions exhibit a significant drop in 2019 in accordance with results from other TD estimates (An et al., 2024; Kim et al., 2021). One possible explanation for this feature is the impact of the U.S. – China trade war, which began in 2018 and reduced China's aluminum production by 4% compared to 2018 (British Geological Survey, 2025). BU CF_4 emission estimates by the International Aluminium Institute (IAI) also exhibit a reduction of 3% from 2018 to 2019 (IAI, 2025). Subsequent high emissions in 2020 and 2021 reflect the increased aluminum production during this time. However, the relative magnitude of the 2019 emission drop in all three TD estimates (approximately 20%) is much larger than the aluminum production drop, and no BU inventory exhibits such an emission drop. While there is also a C_2F_6 emission decrease from 2018 to 2019, it is much less pronounced than for CF_4. Since there is no good explanation for the 2019 CF_4 emission drop, we cannot exclude that it is at least partly an inversion artifact.

According to the IAI's BU emission estimates for 2019 and 2023, China's aluminum industry's PFC emissions increased dramatically during this time. Their data suggests an increase from $3.5\,\mathrm{kt\,yr^{-1}}$ to $6.7\,\mathrm{kt\,yr^{-1}}$ for CF_4 and from $0.16\,\mathrm{kt\,yr^{-1}}$ to $0.21\,\mathrm{kt\,yr^{-1}}$ for C_2F_6 (IAI, 2025). This increase is not represented in our results, likely due to the small number of observations leading to smaller increments in the years 2022 and 2023. When newer measurements will become available in China or East Asia, this possible increase should be revisited.

Comparing our result to other existing emission estimates, we observe good agreement with all TD estimates. Our results match particularly well with those of An et al. (2024), who utilize the largest number of measurements among all previous studies. Results by Arnold et al. (2018) and Kim et al. (2021) exhibit higher interannual variability, likely because their inversions incorporate only measurements from the Gosan station which is located outside of China. The activity-based BU inventory by Guo et al. (2023) agrees relatively well with our results within uncertainties in the second half of the 2010s, but underestimates nearly all TD results significantly before the early 2010s. China's reports to the UNFCCC, as well as EDGAR emission estimates, are much lower throughout the study period, likely underestimating true emissions significantly.

PFC emissions from the 27 current EU countries declined in the late 2000s from $0.86 \pm 0.73\,\mathrm{kt\,yr^{-1}}$ to $0.45 \pm 0.33\,\mathrm{kt\,yr^{-1}}$ (CF_4) and from $0.16 \pm 0.19\,\mathrm{kt\,yr^{-1}}$ to $0.07 \pm 0.09\,\mathrm{kt\,yr^{-1}}$ (C_2F_6) between the early and mid period (Fig. 7). Since the early 2010s, however, emissions stabilized and remained at $0.25 \pm 0.29\,\mathrm{kt\,yr^{-1}}$ (CF_4) and $0.06 \pm 0.08\,\mathrm{kt\,yr^{-1}}$ (C_2F_6) for the late period. The emission decrease is likely the result of efforts by European semiconductor manufacturers to replace C_2F_6 and implement abatement techniques (ESIA, 2001; Say et al., 2021), as well as technological improvements leading to fewer anode effects during aluminum smelting (Tan et al., 2025) and a general shift of the aluminum and electronics industries to Asia.

https://doi.org/10.5194/egusphere-2025-5656
Preprint. Discussion started: 18 December 2025

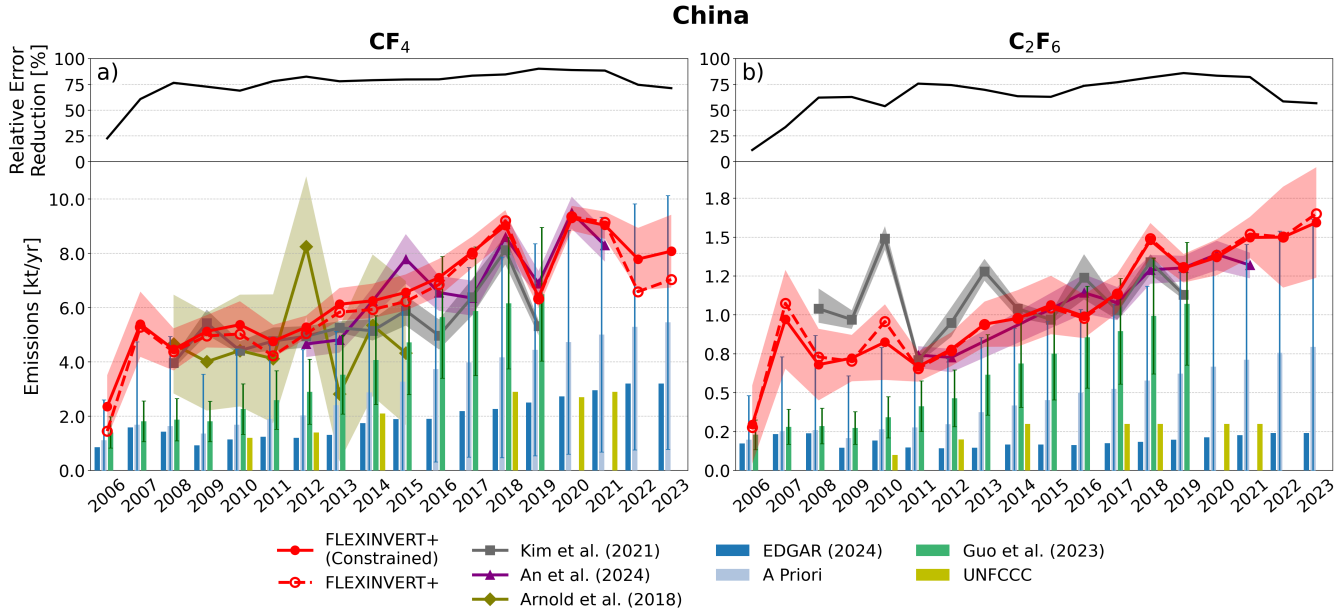

Figure 6. Emissions of CF_4 (a) and C_2F_6 (b) from China for the period 2006 – 2023 from the original BU emission inventory EDGAR (2024) (dark blue bars), our adjusted BU a priori inventory (light blue bars, with assigned a priori uncertainty ranges given by whiskers), the recent regional BU inventory of Guo et al. (2023) (dark green bars, with uncertainty ranges given by whiskers), the UNFCCC (2024a, b) reports (light green bars), our globally constrained inversion results (solid red line with shading indicating uncertainty), our globally unconstrained inversion results (red dashed line), the top-down emissions reported by Kim et al. (2021) (dark grey line with shading indicating uncertainty), by An et al. (2024) (purple line with shading indicating uncertainty), and by Arnold et al. (2018) (green line with shading indicating uncertainty). The relative error reduction by our inversion is shown in the upper panels.

The EU is relatively well covered by measurements since 2006, leading to robust inversion results with little inter-annual variation throughout the whole period. Additionally, a posteriori results remain close to the a priori emissions based on EDGAR, indicating realistic emission magnitudes of the BU estimate for the EU. The EU's emission reports to the UNFCCC are lower than our results on average, particularly during the early period, but remain within uncertainties for nearly all years. Furthermore, our results agree well with results published by Say et al. (2021) for the Benelux region, France, Germany, Ireland, and the United Kingdom, who used the same measurement dataset in Europe but a different transport and inversion model. Within the EU, our results suggest that Romania, as a major aluminum producer, is the largest contributor to the EU's PFC emissions, followed by Germany.

For the first time, we present TD emission estimates for CF_4 and C_2F_6 for the U.S. (Fig. 8). A large number of flask sampling stations across the country makes the U.S. relatively well constrained, particularly for CF_4, resulting in large error reductions. CF_4 emissions remain relatively constant at around $0.37 \pm 0.16\,\mathrm{kt\,yr^{-1}}$ over the whole period, while C_2F_6 emissions declined from $0.21 \pm 0.08\,\mathrm{kt\,yr^{-1}}$ in the early period to $0.15 \pm 0.06\,\mathrm{kt\,yr^{-1}}$ in the mid period to $0.09 \pm 0.03\,\mathrm{kt\,yr^{-1}}$ in the late period.

https://doi.org/10.5194/egusphere-2025-5656
Preprint. Discussion started: 18 December 2025

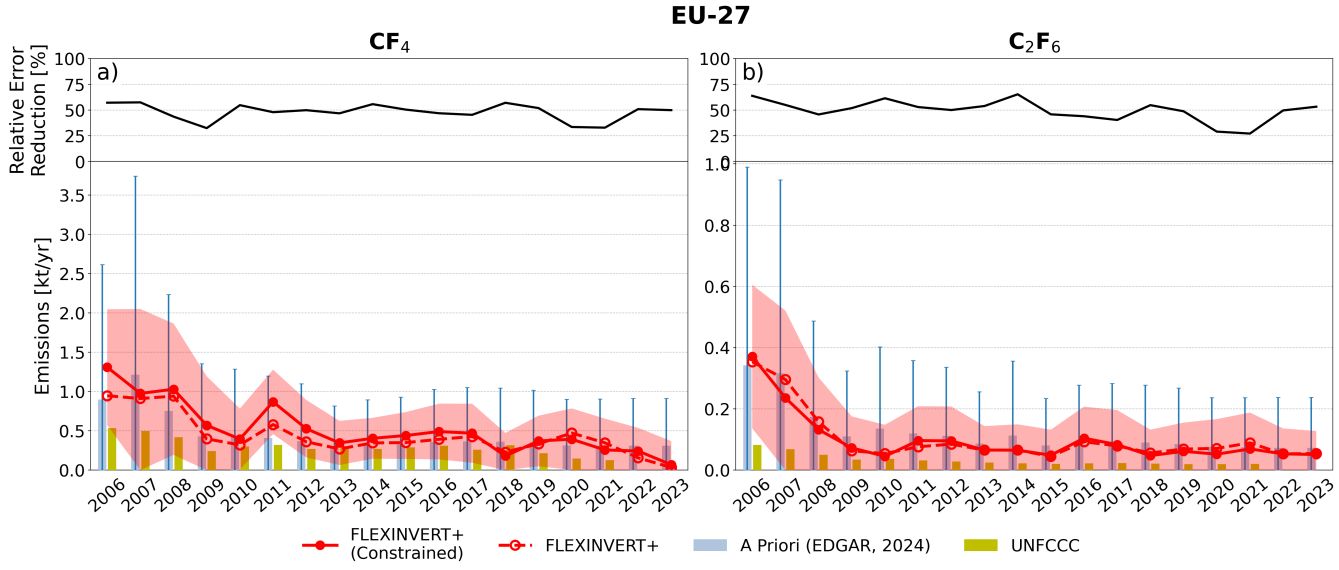

Figure 7. Emissions of CF_4 (a) and C_2F_6 (b) from EU-27 countries for the period 2006 – 2023 from the original BU emission inventory EDGAR (2024) used as our a priori information (light blue bars, with assigned a priori uncertainty ranges given by whiskers), the UNFCCC (2024a, b) reports (light green bars), our globally constrained inversion results (solid red line with shading indicating uncertainty), and our globally unconstrained inversion results (red dashed line). The relative error reduction by our inversion is shown in the upper panels.

These results suggest a shift of emissions from the electronics to the aluminum industry, assuming stable emission ratios, consistent with a phase-out of PFCs in semiconductor manufacturing.

A drop in emissions associated with the global financial crisis is apparent for both gases in 2009, but more pronounced for C_2F_6. This pattern indicates a stronger production decrease by the U.S. electronics industry than the aluminum industry during the crisis. In the U.S., we find the best agreement of our inversion results with both EDGAR and UNFCCC data of all high-emitting regions, indicating that BU reporting in the U.S. is more representative of actual emissions than elsewhere for both species. An exception is the strong emission increase of CF_4 in 2022 and 2023, not apparent in C_2F_6 emissions or BU inventories, and also not supported by electronics or aluminum industry data. We suspect this to be an artifact stemming from a likely underestimation of emissions elsewhere (e.g., notice the drop in emissions in China in fig. 6), and a more uncertain baseline, which are both caused by the much more limited global data coverage in these years. Follow-up studies will be needed when more PFC measurement data become available to clarify whether the increase is an artifact or reflects an actual emission change.

Previous studies suspected a significant fraction of global emissions to originate from regions other than East Asia, Australia, Europe and North America (Kim et al., 2021; Say et al., 2021; Dunse et al., 2019). Results for the South and Southeast Asia (SSEA) region, including aluminum producing countries such as India, Malaysia, Vietnam, and Indonesia as well as large electronics industries in Singapore and Malaysia, are presented here for the first time (Fig. 9). Other countries in the SSEA

https://doi.org/10.5194/egusphere-2025-5656
Preprint. Discussion started: 18 December 2025

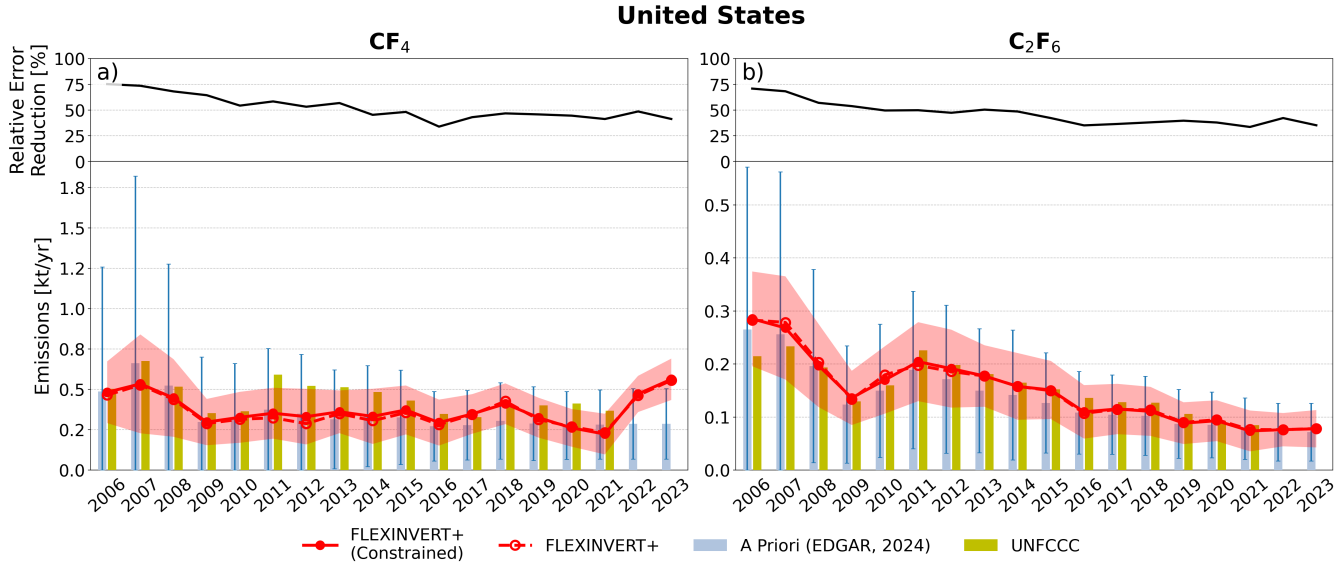

Figure 8. Emissions of CF_4 (a) and C_2F_6 (b) from the United States for the period 2006 – 2023 from the original BU emission inventory EDGAR (2024) used as our a priori information (light blue bars, with assigned a priori uncertainty ranges given by whiskers), the UNFCCC (2024a, b) reports (light green bars), our globally constrained inversion results (solid red line with shading indicating uncertainty), and our globally unconstrained inversion results (red dashed line). The relative error reduction by our inversion is shown in the upper panels.

region are assumed to have negligible PFC emissions due to the absence of large aluminum or electronics industries. The emission sensitivity in this region is particularly low (see Fig. 3) as there are no measurement stations within the region itself, leading to small error reductions and highly uncertain posterior emissions. Nonetheless, large positive deviations from a priori emissions are obtained for both species over the whole study period, indicating that BU emissions possibly underestimate actual emissions.

CF_4 emissions in the SSEA region rose continuously from $0.62 \pm 0.70\,\mathrm{kt\,yr^{-1}}$ in the early period to $1.41 \pm 1.03\,\mathrm{kt\,yr^{-1}}$ in the mid period and $3.39 \pm 1.26\,\mathrm{kt\,yr^{-1}}$ in the late period, corresponding to around $22 \pm 9\%$ of global total emissions. Emissions of C_2F_6 experienced an increase from $0.21 \pm 0.30\,\mathrm{kt\,yr^{-1}}$ in the early period to $0.35 \pm 0.37\,\mathrm{kt\,yr^{-1}}$ in the mid period, and rose further to $0.42 \pm 0.36\,\mathrm{kt\,yr^{-1}}$ in the late period, representing $18 \pm 15\%$ of global emissions. C_2F_6 emissions, however, exhibit more inter-annual variability, even lower error reduction as well as larger relative uncertainty than CF_4 emissions.

The EDGAR dataset suggests much lower emissions compared to our results and only accounts for approximately 18% of the region's TD emissions in the most recent period for both CF_4 and C_2F_6. The cause for EDGAR's low values is mainly extremely low estimates for India. Emission reporting of both species' emissions to the UNFCCC is sparse in this region and consists mainly of India's reports in 2010, 2014, 2016, and 2020. It appears that these reports overestimate India's emissions for 2010, 2014, and 2016, since these are higher than our inversion results for the entire SSEA region. We assume the reported

https://doi.org/10.5194/egusphere-2025-5656
Preprint. Discussion started: 18 December 2025

value for 2020, when a refined method was applied, to be more realistic, as its magnitude is similar to reports of countries with similar-sized aluminum industries (MoEFCC, 2024).

Our inversion results for the SSEA region demonstrate the benefit of constraining the total global emissions of our regionally resolving model toward well-known global emission values for regional emission analysis. Particularly for CF_4, the constrained FLEXINVERT+ inversion result exhibits a much more continuous emission increase than the unconstrained inversion, which shows large – and likely unrealistic – inter-annual variability. This indicates that if a major emitting region is not well constrained by measurements, the additional information of the global emission sum can help to constrain emissions in that region and stabilize the inversion results. Nevertheless, it is clear that uncertainties remain high in such a region.

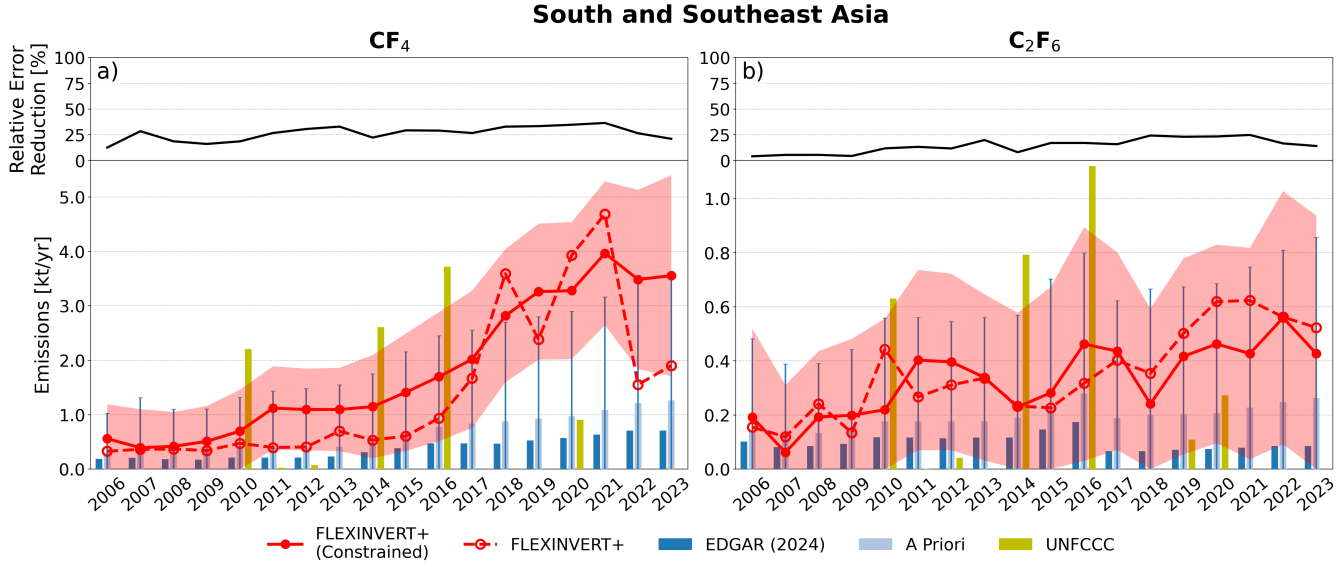

Figure 9. Emissions of CF_4 (a) and C_2F_6 (b) from South and Southeast Asia for the period 2006 – 2023 from the original BU emission inventory EDGAR (2024) (dark blue bars), our adjusted BU a priori inventory (light blue bars, with assigned a priori uncertainty ranges given by whiskers), the UNFCCC (2024a, b) reports (light green bars), our globally constrained inversion results (solid red line with shading indicating uncertainty), and our globally unconstrained inversion results (red dashed line). The relative error reduction by our inversion is shown in the upper panels.

3.3 Reassessment of the top-down to bottom-up emission discrepancy

Figure 10 presents the fractional contributions of several countries and regions to the global discrepancy between our constrained inversion result and the EDGAR BU inventory, referred to as TD – BU discrepancy. It is important to note that these values depend strongly on the chosen BU inventory. We chose EDGAR for comparison, as it presents the only global dataset. For instance, if we compared China's TD emissions to the BU dataset compiled by Guo et al. (2023) instead of EDGAR, its fraction of the global discrepancy would be significantly lower.

https://doi.org/10.5194/egusphere-2025-5656
Preprint. Discussion started: 18 December 2025

China is by far the largest contributor to the global TD – BU discrepancy at $84 \pm 19\%$, $79 \pm 9\%$, and $61 \pm 11\%$ for CF_4 and $63 \pm 31\%$, $77 \pm 13\%$, and $70 \pm 15\%$ for C_2F_6. China's fractional contribution is also larger than its absolute emission share, indicating that EDGAR estimates in China are particularly far off from our TD results. In the early period, China is followed by South Korea, Russia, and India for CF_4 and by South Korea, Japan, Malaysia+Singapore, and India for C_2F_6. The high discrepancies in South Korea and Japan likely result from substantial underestimation of PFC emissions from their electronics industries in the EDGAR inventory.

In the mid period, China's contribution to the TD – BU discrepancy is followed by that of India and South Korea for both species. In the late period, the contribution from India and the Malaysia+Singapore region combined increased to $23 \pm 17\%$ for CF_4 and $25 \pm 27\%$ for C_2F_6, contributing significantly to closing the global TD – BU gap. The CF_4 TD – BU discrepancy is therefore primarily closed by aluminum-producing regions. In contrast, the TD – BU discrepancy of C_2F_6 was initially closed by primarily electronics-producing regions in the early period, but shifted toward aluminum-producing regions in the late period as well. Notably, a negative discrepancy is observed in Canada, which hosts a relatively large aluminum industry. EDGAR estimates Canada's emissions to be much higher than our posterior results, possibly because it applies general emission factors, unsuitable to Canada's relatively efficient aluminum smelters (Tan et al., 2025).

In general, this analysis shows that the EDGAR BU inventory significantly underestimates emissions not only in China but also in India and Malaysia+Singapore. With steadily rising emissions and growing aluminum and electronics industries in these regions, it is crucial to improve BU inventories and expand industry and government reporting, particularly in the rapidly developing SSEA region. It is also essential to build up measurement capacity in this region to reduce the large uncertainties in TD estimates.

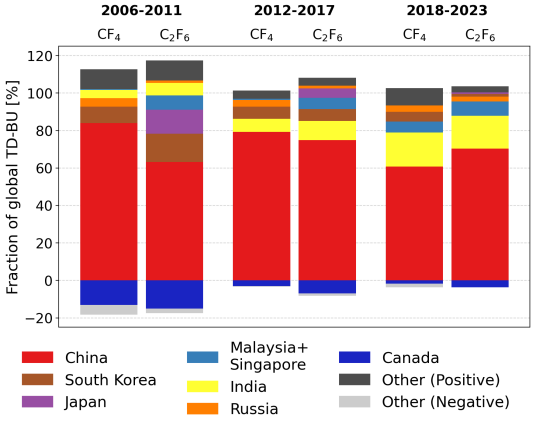

Figure 10. Fractional contributions of individual countries to the top-down to bottom-up global emission discrepancy obtained between our globally constrained inversion result and the EDGAR inventory for CF_4 and C_2F_6, respectively, and for three inversion periods.

https://doi.org/10.5194/egusphere-2025-5656
Preprint. Discussion started: 18 December 2025

3.4 Emission contribution by industry

Using the C_2F_6/CF_4 emission ratio approach introduced by Kim et al. (2014), we split emissions into contributions from the aluminum and electronics industries. A higher ratio ($0.4\,kg\,kg^{-1}$) indicates predominant emissions from electronics manufacturing, while a lower ratio ($0.1\,kg\,kg^{-1}$) is associated with emissions from aluminum smelting. However, large uncertainties exist due to a wide range of manufacturing methods in both industries, changes in manufacturing techniques over time, and other PFC sources. Assuming constant emission ratios regionally and temporally, we present country-level and grid point-level emissions per industry averaged over the late period (2018 – 2023).

For our inversion results and the EDGAR BU inventory, figure 11 shows emission ratios and industry-level CF_4 and C_2F_6 emissions for the largest PFC-emitting regions, as well as globally. While the difference between our FLEXINVERT+ results and EDGAR are generally small, there are notable differences in several regions. Globally, the inversion increases the average emission ratio from $0.13\,kg\,kg^{-1}$ in EDGAR to $0.16\,kg\,kg^{-1}$. Our results indicate higher contribution by the aluminum smelting industry at 81% for CF_4 and increased contribution by the electronics industry at 48% for C_2F_6, compared to EDGAR. Regions with dominant aluminum industries, such as India and Russia exhibit low C_2F_6/CF_4 ratios. Similarly, for Canada, the inversion yields a very low C_2F_6/CF_4 ratio, whereas the EDGAR inventory shows a relatively high ratio. The discrepancy is likely attributable to Canada's modern and efficient smelting technology, which does not seem to be fully accounted for in the EDGAR dataset. Predominantly electronics manufacturing regions such as Japan, South Korea, and Taiwan exhibit strongly varying emission ratios from $0.58\,kg\,kg^{-1}$ (Japan) to $0.05\,kg\,kg^{-1}$ (South Korea). For South Korea and Taiwan, where there are no active aluminum smelters, the resulting industry contributions in panels b) and c) are unrealistic as a result of our simplified industry emission ratios. In South Korea, the emission ratio was much higher at $0.41\,kg\,kg^{-1}$ during the early period (2006 – 2011) and decreased throughout the 2010s. A possible explanation could be a phase-out of C_2F_6 by the electronics industry, whereas CF_4 may still be more widely used. A similar development, though to a smaller extent, occurred in Japan ($0.83\,kg\,kg^{-1}$ to $0.59\,kg\,kg^{-1}$) and Taiwan ($0.36\,kg\,kg^{-1}$ to $0.23\,kg\,kg^{-1}$), further supporting this hypothesis. The remaining regions of China, Malaysia and Singapore, the U.S., and the EU exhibit both significant aluminum and electronics industries, which are represented by emissions ratios between $0.1\,kg\,kg^{-1}$ and $0.4\,kg\,kg^{-1}$. Generally, in these regions, CF_4 is predominantly emitted by their aluminum and C_2F_6 by their electronics industries. In China, the emission ratio underwent a relatively large adjustment from the EDGAR data to our inversion results, with an increase from $0.08\,kg\,kg^{-1}$ to $0.18\,kg\,kg^{-1}$. For CF_4, the aluminum industry represents the largest contribution at 75%, while for C_2F_6, the electronics industry is responsible for the majority of emissions at 58%. For C_2F_6, the electronics industry's share is much larger compared to the EDGAR estimate.

For the U.S. and southern Canada, figure 12 presents the distribution of regional emission ratios for grid cells that exceed the 95th percentile of both CF_4 and C_2F_6 emissions (a) and CF_4 emissions (b) for the late period (2018 – 2023). Additionally, locations of publicly known aluminum smelters and electronics manufacturing facilities as listed by EPA (2025) and Wikipedia (2025a, b) are presented in figure 12. We note that it is difficult to determine whether the presented industry locations were active PFC emitters during the late period. This is particularly true for the electronics industry, as not all fabrication plants inherently use and emit PFCs.

https://doi.org/10.5194/egusphere-2025-5656
Preprint. Discussion started: 18 December 2025

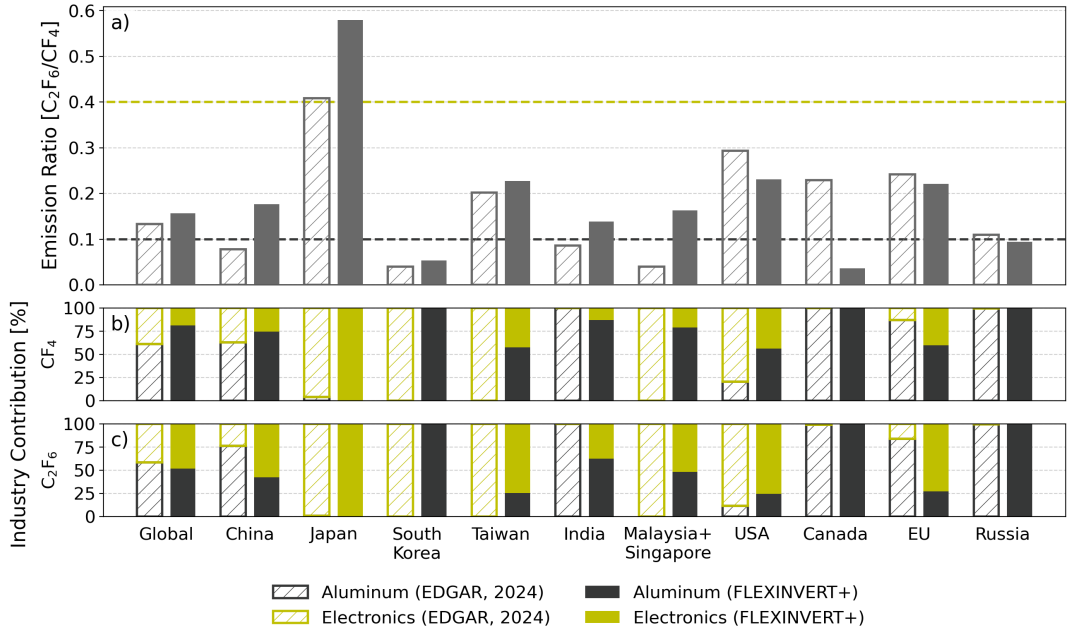

Figure 11. Emission ratio C_2F_6/CF_4 (a) as well as derived relative emission contributions from the aluminum and electronics industry for CF_4 (b) and C_2F_6 (c) for the whole globe as well as for selected countries or regions, based on EDGAR bottom-up industry specific estimates (hatched boxes) and our globally constrained top-down estimates (shaded boxes), for the period 2018 – 2023.

In line with the assumed emission ratio for each industry, grid cells with high ratios should generally correspond to electronics manufacturers, while those with low ratios should correspond to aluminum smelters. Additionally, many industry locations overlap well with high emission grid cells, however, the opposite is not necessarily true, as high values in the emissions do not necessarily correspond to known industry locations (e.g. 42°N 88°W, Chicago). The emission distribution of our inversion results is partly informed by EDGAR-based a priori emissions, which themselves are likely based on industry locations and possibly other proxy data such as population density (at least in the U.S.). This is, however, difficult to confirm due to the lack of detailed documentation of the EDGAR dataset. Also notice the large change of C_2F_6/CF_4 emission ratios by the inversion for Canada (Fig. 11), which demonstrates a strong measurement constraint.

Very high emissions are present in southeast Canada, where several large aluminum smelters in Sept-Îles, Alma, and Bécancour produce roughly three times the amount of the whole U.S. aluminum industry in recent years (British Geological Survey, 2025). This is reflected in comparably low emissions at aluminum smelters in the U.S.. Emissions, particularly of C_2F_6, are dominated by the electronics industry (see Fig. 11) primarily along the west coast and in central Texas. Notice the co-location of high-emission grid cells with high C_2F_6/CF_4 emission ratios, with the known electronic industry locations in the western U.S..

Figure 13 presents the gridded emission ratios (a) and CF_4 emissions (b) averaged over the late period (2018 – 2023) over Europe. Locations of publicly known aluminum smelters, electronics manufacturers, and chemical or other PFC-emitting fa-

https://doi.org/10.5194/egusphere-2025-5656
Preprint. Discussion started: 18 December 2025

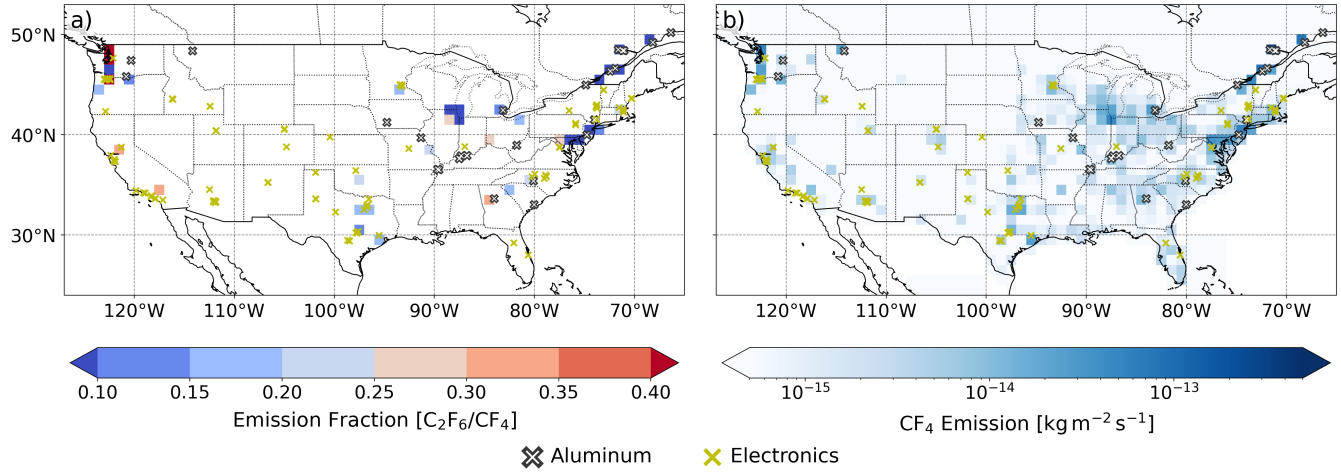

Figure 12. C_2F_6/CF_4 emission ratio (a) and CF_4 emissions (b) in North America for the period 2018-2023. Also shown are the known locations of aluminum smelters (black crosses) and electronics factories (yellow crosses).

cilities are compiled from the European Environment Agency (2025) and Wikipedia (2025a, b). Again, note that locations of active PFC emitters are possibly outdated or incomplete due to difficulties in determining and verifying actual locations. Many emission sources with low C_2F_6/CF_4 ratios overlap with known aluminum smelters. The largest aluminum smelters in Europe are located in Norway and are highly efficient, leading to significantly lower PFC emissions per produced unit of aluminum, similar to Canada's smelting industry (Tan et al., 2025). Other large aluminum smelters are situated in Spain, the Ruhr region in Germany, Sweden, Slovakia, Turkey, Greece, and Russia, all of which exhibit emission ratios lower than $0.2\,\mathrm{kg\,kg^{-1}}$. Aluminum smelters in Romania and Slovenia, emit substantial amounts of PFCs, but exhibit relatively high emission ratios larger than $0.25\,\mathrm{kg\,kg^{-1}}$. Emissions from electronics manufacturers are generally well captured by the inversion, for instance, near Paris (France), the Netherlands, northern Italy, across multiple regions in Germany, and Saint Petersburg (Russia), but their magnitudes are, on average, lower than those of the aluminum industry. According to Say et al. (2021), C_2F_6 emissions by an electronics manufacturer near Dublin in Ireland ceased by 2012, however, our results still indicate PFC emissions in that region with a relatively low emission ratio under $0.2\,\mathrm{kg\,kg^{-1}}$. Most chemical and other PFC-emitting facilities listed by the European Environment Agency (2025) emit relatively small amounts compared to aluminum and electronics sources. Only one chemical manufacturer in northern Belgium emits significant quantities and is the largest source of PFCs in the Benelux region. Say et al. (2021) also found this facility to be a dominant source of CF_4 and C_2F_6 in 2012.

Figure S5 shows spatial maps of emission ratio and CF_4 emissions for large parts of Asia. Given the extensive research on PFC emissions in China and the high uncertainty of results in other parts of Asia, we do not go into the details of sub-national distributions and industry contributions.

https://doi.org/10.5194/egusphere-2025-5656
Preprint. Discussion started: 18 December 2025

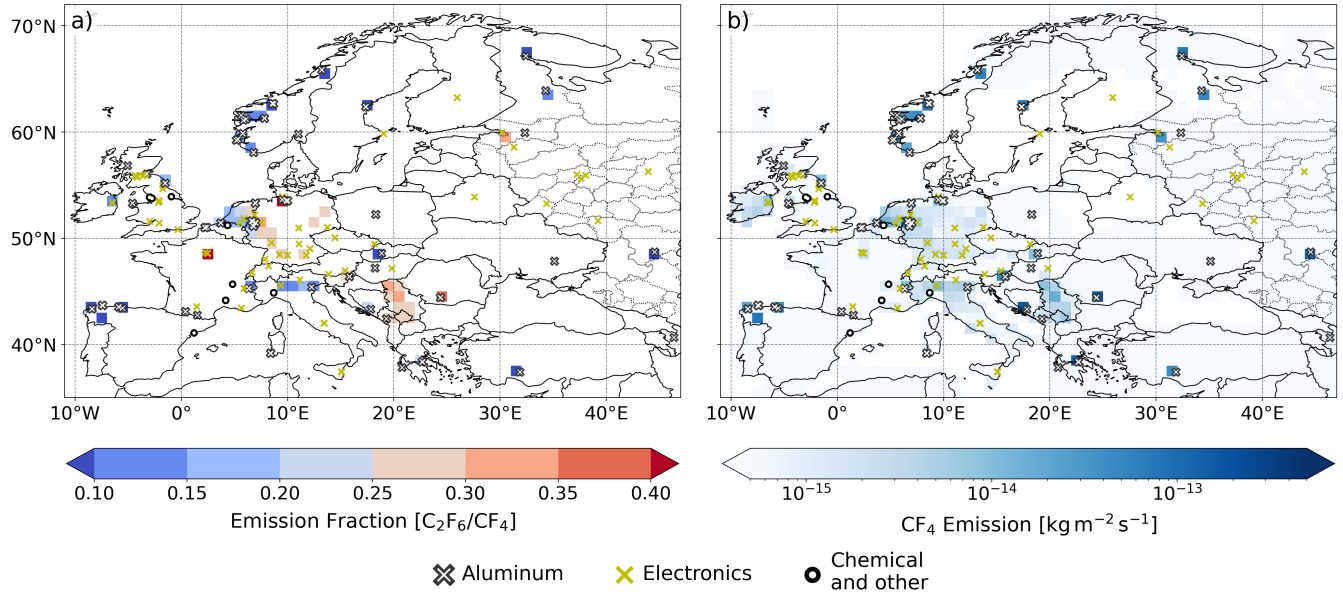

Figure 13. C_2F_6/CF_4 emission ratio (a) and CF_4 emissions (b) in Europe for the period 2018 – 2023. Also shown are the known locations of aluminum smelters (black crosses), electronics factories (yellow crosses), and other major sources (black dots).

4 Conclusions

Using the FLEXPART transport model and the FLEXINVERT+ inversion framework, we performed the first regionally resolved global inversion of the perfluorocarbons tetrafluoromethane (CF_4, PFC-14) and hexafluoroethane (C_2F_6, PFC-116) to provide top-down estimates of their emissions. The inversions were performed annually for the period 2006 to 2023, although results for the first year and the last two years must be interpreted with caution because of the poor measurement coverage in these years. Our main findings from this study are:

- The introduction of a novel constraint on the global emission total brings the global emission total of our regionally resolved emissions into close agreement with the relatively well known global emissions obtained from box model calculations. While the uncertainties in poorly monitored regions such as South and Southeast Asia remain high, the posterior emissions for these regions show substantially less inter-annual variability than without the global constraint. This indicates that the inversion is stabilized by the global total constraint and suggests that results for these regions are meaningful within their large posterior uncertainties. The additional global constraint has little impact on the results in well-monitored regions such as Europe, North America, or China.

- The inversion increased the global CF_4 and C_2F_6 emissions substantially compared to our prior emissions, which were based mainly on the EDGAR data set, with adjustments for India, China and South Korea. For the period 2018 – 2023,

https://doi.org/10.5194/egusphere-2025-5656
Preprint. Discussion started: 18 December 2025

our posterior emissions are 2.6 ± 0.3 and 3.1 ± 0.7 times higher than the prior emissions for CF_4 and C_2F_6, respectively. The relative differences compared to the unadjusted EDGAR inventory and the UNFCCC reports are even larger.

- China is the main emitter of both CF_4 and C_2F_6, with relative contributions of 56% and 58%, respectively, during the period 2018 – 2023. While China's contribution to CF_4 emissions increased in the 2000s, it stabilized in the 2010s and early 2020s. In contrast, China's contribution to C_2F_6 emissions increased throughout the period, explainable by the continuous growth of the Chinese electronics industry.

- The EDGAR inventory underestimates the Chinese emissions substantially throughout the entire inversion period, accounting for most of the discrepancy between global top-down versus bottom-up emissions. In contrast, the Chinese inventory of Guo et al. (2023), while still having somewhat lower emissions, agrees within uncertainties with our inversion results. We also find good agreement with previous inversion studies for China (Arnold et al., 2018; Kim et al., 2021) and particularly with the study of An et al. (2024), which was based on the largest measurement data set.

- India's emissions are highly uncertain because of a lack of measurement data in the region. However, while India's emissions appear to contribute marginally to global emissions at the beginning of our inversion period, its contribution increases to 12 – 13% toward the end for both species, which would make India the second largest emitter after China. Also, other countries in South and Southeast Asia appear to have an increasing contribution to the global PFC emissions, making it a key region to monitor in the future.

- For Europe, a region relatively well constrained by measurements, our inversion results stay close to the a priori EDGAR emissions, whereas the UNFCCC reports tend to underestimate Europe's emissions. The emissions of both PFCs decreased from 2006 to 2010, with little changes in later years.

- For the United States, another well constrained region, our inversion results also remain relatively close to the a priori EDGAR inventory and are also in good agreement with the UNFCCC reports. While there was relatively little change in CF_4 emissions, emissions of C_2F_6 decreased continuously from 2006 to 2023, except for a temporary emission drop in 2009, which is likely related to the global financial crisis.

- Compared to EDGAR's industry level estimates, our results suggest greater contribution by the aluminum industry to CF_4 emissions at 81% and increased contribution by the electronics industry to C_2F_6 emissions at 48%. We find relatively good agreement of the spatial distribution of the C_2F_6/CF_4 emission ratios with known locations of aluminum smelters and electronics factories in North America and Europe.

Code availability. The used FLEXINVERT+ code (described in detail by Thompson and Stohl, 2014) is provided at https://doi.org/10.25365/phaidra.488. The source code of FLEXPART11 including the linear chemistry module (LCM) is available at https://zenodo.org/records/13748655 (Bakels et al., 2024).

https://doi.org/10.5194/egusphere-2025-5656
Preprint. Discussion started: 18 December 2025

Data availability. CF_4 and C_2F_6 annual emission fields between 2006 and 2023 are provided at https://doi.org/10.25365/phaidra.751. Daily-resolved global CF_4 and C_2F_6 mole fraction fields between 2006 and 2023 are provided at https://doi.org/10.25365/phaidra.752. Atmospheric mole fraction measurements of CF_4 and C_2F_6 used in this study are freely available from the following sources: AGAGE data at https://doi.org/10.60718/0FXA-QF43; NOAA data at https://doi.org/10.15138/1sds-1672; Xichong data at https://doi.org/10.7910/DVN/BFINPM; Trollhaugen data at https://doi.org/10.48597/P8CA-KWZG; CMA data at https://doi.org/10.1073/pnas.2400168121

Author contributions. BP, MV, LK and AS designed the study. BP and LK performed the FLEXPART, FLEXPART LCM, and FLEXINVERT+ simulations. MV helped with FLEXPART and FLEXINVERT+ setup and simulation issues. Measurement data was provided by MC, AE, PBK, CRL, JM, SO'D, RGP, KMS, IV, MKV, TW, RFW and DY. BP, MV and AS wrote the manuscript and created the figures with input from all co-authors.

Competing interests. The authors declare that they have no conflict of interest.

Acknowledgements. Andreas Stohl and Martin Vojta were partly supported by the Horizon Europe projects EYE-CLIMA (grant no. 101081395) and Edu4Climate (101071247). We thank the whole AGAGE team for providing high frequency measurement data. Operation of the American Samoa observatory (SMO) is funded by the National Oceanic and Atmospheric Administration (NOAA) in the USA. AGAGE operations at SMO and Trinidad Head are funded by the National Aeronautics and Space Administration (NASA) in the USA. The Kennaook/Cape Grim station is funded and managed by the Australian Bureau of Meteorology, with the AGAGE scientific program jointly managed with the Commonwealth Scientific and Industrial Research Organization (CSIRO). Support is also received from the Australian Department of Climate Change, Energy, the Environment and Water (DCCEEW), Refrigerant Reclaim Australia (RRA), and through the NASA Upper Atmospheric Research Program award to MIT (80NSSC21K1369) with a sub-award to CSIRO for Kennaook/Cape Grim AGAGE activities. AGAGE operations at Ragged Point are currently supported by the National Aeronautic and Space Administration (NASA) Grant 80NSSC21K1369 (to MIT, under sub-award S5608 to the University of Bristol) with additional funding from the National Oceanic and Atmospheric Administration (NOAA) Contract 1305M319CNRMJ0028 (to the University of Bristol). Taunus Observatory is funded by BMBF through the ACTRIS-D project (FKZ 01LK2001I). Halocarbon measurements are funded by the European Commission as part of the PARIS project (GA 101081430). Monte Cimone is funded by the CNR-ISAC (National Research Council of Italy Institute of Atmospheric Sciences and Climate) and PON PER-ACTRIS-IT (Programma Operativo Nazionale Ricerca e Innovazione 2014-2020, Potenziamento della componente italiana dell'Infrastruttura di Ricerca Aerosol, Clouds and Trace Gases Research). Atmospheric gas measurements at Mace Head are supported by research grants from the Department of Energy, Security and Net Zero (DESNZ), contract number prj_1604 in the UK; and the National Aeronautic and Space Administration Grants (NASA), sub-award S5608 PO# - 752393. Observations at the Gosan station are supported by the Basic Science Research Program through the National Research Foundation of Korea (NRF) funded by the Ministry of Education (no. NRF-2016R1A2B2010663). The halocarbon measurements at Zeppelin Observatory are funded by the Norwegian Environment Agency. Financial support for the AGAGE measurements at Jungfraujoch is provided by the Swiss National Programs HALCLIM and

https://doi.org/10.5194/egusphere-2025-5656
Preprint. Discussion started: 18 December 2025

CLIMGAS-CH (Swiss Federal Office for the Environment [FOEN]) and by the International Foundation High Altitude Research Stations Jungfraujoch and Gornergrat (HFSJG).

This research was supported in part by the NOAA cooperative agreement NA22OAR4320151. The statements, findings, conclusions, and recommendations are those of the author(s) and do not necessarily reflect the views of NOAA or the U.S. Department of Commerce.

Trollhaugen measurement data used in this study were accessed from EBAS (https://ebas.nilu.no) hosted by NILU. Specifically, the use included data affiliated with the framework: NILU, GAW-WDCRG. We thank Yuyang Chen and Lei Zhu for providing PFC measurement at Xichong Station, Shenzhen, China. We also thank Bo Yao and the CMA for operating a PFC measurement network in China and providing data.

We are grateful to Omid Nabavi, Marina Dütsch, Lucie Bakels (University of Vienna), and Christina Groot Zwaaftink (NILU) for their technical assistance and constructive discussions. We further thank Jooil Kim (Scripps Institution of Oceanography), Petra Seibert (University of Vienna), Rona Thompson (NILU), Alistair Manning (Met Office Hadley Centre), and Matthew Rigby (University of Bristol) for valuable scientific discussions and their input.

https://doi.org/10.5194/egusphere-2025-5656
Preprint. Discussion started: 18 December 2025

References

An, M., Prinn, R. G., Western, L. M., Yao, B., Zhao, X., Kim, J., Mühle, J., Chi, W., Harth, C. M., Hu, J., Ganesan, A. L., and Rigby, M.: Substantial increase in perfluorocarbons CF4 (PFC-14) and C2F6 (PFC-116) emissions in China, Proceedings of the National Academy of Sciences, 121, e2400168 121, https://doi.org/10.1073/pnas.2400168121, 2024.

Arnold, T., Manning, A. J., Kim, J., Li, S., Webster, H., Thomson, D., Mühle, J., Weiss, R. F., Park, S., and O'Doherty, S.: Inverse modelling of CF_4 and NF_3 emissions in East Asia, Atmospheric Chemistry and Physics, 18, 13 305–13 320, https://doi.org/10.5194/acp-18-13305-2018, 2018.

Bakels, L., Tatsii, D., Tipka, A., Thompson, R., Dütsch, M., Blaschek, M., Seibert, P., Baier, K., Bucci, S., Cassiani, M., Eckhardt, S., Groot Zwaaftink, C., Henne, S., Kaufmann, P., Lechner, V., Maurer, C., Mulder, M. D., Pisso, I., Plach, A., Subramanian, R., Vojta, M., and Stohl, A.: FLEXPART version 11: improved accuracy, efficiency, and flexibility, Geoscientific Model Development, 17, 7595–7627, https://doi.org/10.5194/gmd-17-7595-2024, 2024.

Bergamaschi, P., Segers, A., Brunner, D., Haussaire, J.-M., Henne, S., Ramonet, M., Arnold, T., Biermann, T., Chen, H., Conil, S., Delmotte, M., Forster, G., Frumau, A., Kubistin, D., Lan, X., Leuenberger, M., Lindauer, M., Lopez, M., Manca, G., Müller-Williams, J., O'Doherty, S., Scheeren, B., Steinbacher, M., Trisolino, P., Vítková, G., and Yver Kwok, C.: High-resolution inverse modelling of European CH4 emissions using novel FLEXPART-COSMO TM5 4DVAR inverse modelling system, Atmospheric Chemistry and Physics, https://doi.org/10.5194/acp-2022-118, 2022.

British Geological Survey: World mineral statistics archive, https://www.bgs.ac.uk/mineralsuk/statistics/world-mineral-statistics/world-mineral-statistics-archive/, 2025.

Cai, B., Liu, H., Kou, F., Yang, Y., Yao, B., Chen, X., Wong, D. S., Zhang, L., Li, J., Kuang, G., Chen, L., Zheng, J., Guan, D., and Shan, Y.: Estimating perfluorocarbon emission factors for industrial rare earth metal electrolysis, Resources, Conservation and Recycling, 136, 315–323, https://doi.org/10.1016/j.resconrec.2018.04.018, 2018.

Calvo Buendia, E., Tanabe, K., Kranjc, A., Jamsranjav, B., Fukuda, M., Ngarize, S., Osako, A., Pyrozhenko, Y., Shermanau, P., and Federici, S.: 2019 Refinement to the 2006 IPCC Guidelines for National Greenhouse Gas Inventories, IPCC, Switzerland, https://www.ipcc-nggip.iges.or.jp/public/2019rf/index.html, 2019.

Chen, Y.: Available Data for "Inverse Modeling of High Global Warming Potential Perfluorinated Greenhouse Gases in Southeastern China", https://doi.org/10.7910/DVN/BFINPM, 2025.

Chen, Y., Yao, B., An, M., Ding, A., Liu, S., Li, X., Li, Y., O'Doherty, S., Krummel, P. B., Yang, H., Yu, H., Chen, L., Yang, X., Fu, T.-M., Shen, H., Ye, J., Wang, C., and Zhu, L.: Emissions of Perfluorinated Greenhouse Gases in Southeastern China Derived From High-Frequency In Situ Observations, Geophysical Research Letters, 52, e2024GL111 393, https://doi.org/10.1029/2024GL111393, 2025.

Cicerone, R. J.: Atmospheric Carbon Tetrafluoride: A Nearly Inert Gas, Science, 206, 59–61, https://doi.org/10.1126/science.206.4414.59, 1979.

Czerniak, M.: PFC Emission Reduction in the Semiconductor Industry, in: Light Metals 2018, edited by Martin, O., pp. 1495–1498, Springer International Publishing, Cham, https://doi.org/10.1007/978-3-319-72284-9_195, 2018.

Dunse, B. L., Derek, N., Fraser, P. J., Krummel, P. B., and Steele, L. P.: Australian and global HFC, PFC, Sulfur Hexafluoride, Nitrogen Trifluoride and Sulfuryl Fluoride Emissions, CSIRO Oceans and Atmosphere, 2019.

https://doi.org/10.5194/egusphere-2025-5656
Preprint. Discussion started: 18 December 2025

EDGAR: (Emissions Database for Global Atmospheric Research), Community GHG Database, a collaboration between the European Commission, Joint Research Centre (JRC), the International Energy Agency (IEA), and comprising IEA-EDGAR CO2, EDGAR CH4, EDGAR N2O, EDGAR F-gases version 2024 European Commission, JRC (Datasets), https://edgar.jrc.ec.europa.eu/dataset_ghg2024, 2024.

EPA: EPA Facility Level GHG Emissions Data, https://ghgdata.epa.gov/ghgp/main.do, 2025.

ESIA: PFC Voluntary Agreement Report, Tech. rep., https://www.eusemiconductors.eu/sites/default/files/uploads/20111214_ESIA_PerfluoroBrochure.pdf, 2001.

European Environment Agency: European Pollutant Release and Transfer Register, https://www.eea.europa.eu/data-and-maps/data/member-states-reporting-art-7-under-the-european-pollutant-release-and-transfer-register-e-prtr-regulation-23/european-pollutant-release-and-transfer-register-e-prtr-data-base/eprtr_v9_csv.zip, 2025.

Guo, L. and Fang, X.: Revealing the global emission gaps for fully fluorinated greenhouse gases, Scientific Reports, 14, 8753, https://doi.org/10.1038/s41598-024-58504-x, 2024.

Guo, L., Yang, Y., Fraser, P. J., Velders, G. J. M., Liu, Z., Cui, D., Quan, J., Cai, Z., Yao, B., Hu, J., and Fang, X.: Projected increases in emissions of high global warming potential fluorinated gases in China, Communications Earth & Environment, 4, 1–9, https://doi.org/10.1038/s43247-023-00859-6, 2023.

Henne, S., Brunner, D., Oney, B., Leuenberger, M., Eugster, W., Bamberger, I., Meinhardt, F., Steinbacher, M., and Emmenegger, L.: Validation of the Swiss methane emission inventory by atmospheric observations and inverse modelling, Atmospheric Chemistry and Physics, 16, 3683–3710, https://doi.org/10.5194/acp-16-3683-2016, 2016.

Hersbach, H., Bell, B., Berrisford, P., Hirahara, S., Horányi, A., Muñoz-Sabater, J., Nicolas, J., Peubey, C., Radu, R., Schepers, D., Simmons, A., Soci, C., Abdalla, S., Abellan, X., Balsamo, G., Bechtold, P., Biavati, G., Bidlot, J., Bonavita, M., De Chiara, G., Dahlgren, P., Dee, D., Diamantakis, M., Dragani, R., Flemming, J., Forbes, R., Fuentes, M., Geer, A., Haimberger, L., Healy, S., Hogan, R. J., Hólm, E., Janisková, M., Keeley, S., Laloyaux, P., Lopez, P., Lupu, C., Radnoti, G., de Rosnay, P., Rozum, I., Vamborg, F., Villaume, S., and Thépaut, J.-N.: The ERA5 global reanalysis, Quarterly Journal of the Royal Meteorological Society, 146, 1999–2049, https://doi.org/10.1002/qj.3803, 2020.

Hodnebrog, O., Aamaas, B., Fuglestvedt, J. S., Marston, G., Myhre, G., Nielsen, C. J., Sandstad, M., Shine, K. P., and Wallington, T. J.: Updated Global Warming Potentials and Radiative Efficiencies of Halocarbons and Other Weak Atmospheric Absorbers, Reviews of Geophysics, 58, https://doi.org/10.1029/2019RG000691, 2020.

IAI: 2019 Anode Effect Survey Report, Tech. rep., https://international-aluminium.org/resources/2019-anode-effect-survey-report/, 2020.

IAI: Primary Aluminium Production, https://archive.international-aluminium.org/statistics/primary-aluminium-production/, 2021.

IAI: Perfluorocarbon (PFC) Emissions, https://international-aluminium.org/statistics/perfluorocarbon-pfc-emissions/, 2025.

Illuzzi, F. and Thewissen, H.: Perfluorocompounds emission reduction by the semiconductor industry, Journal of Integrative Environmental Sciences, 7, 201–210, https://doi.org/10.1080/19438151003621417, 2010.

IPCC: Climate Change 2021 – The Physical Science Basis: Working Group I Contribution to the Sixth Assessment Report of the Intergovernmental Panel on Climate Change, Cambridge University Press, Cambridge, https://doi.org/10.1017/9781009157896, 2023.

Kim, J., Fraser, P. J., Li, S., Mühle, J., Ganesan, A. L., Krummel, P. B., Steele, L. P., Park, S., Kim, S.-K., Park, M.-K., Arnold, T., Harth, C. M., Salameh, P. K., Prinn, R. G., Weiss, R. F., and Kim, K.-R.: Quantifying aluminum and semiconductor industry perfluorocarbon emissions from atmospheric measurements, Geophysical Research Letters, 41, 4787–4794, https://doi.org/10.1002/2014GL059783, 2014.

https://doi.org/10.5194/egusphere-2025-5656
Preprint. Discussion started: 18 December 2025

Kim, J., Thompson, R., Park, H., Bogle, S., Mühle, J., Park, M.-K., Kim, Y., Harth, C. M., Salameh, P. K., Schmidt, R., Ottinger, D., Park, S., and Weiss, R. F.: Emissions of Tetrafluoromethane (CF4) and Hexafluoroethane (C2F6) From East Asia: 2008 to 2019, Journal of Geophysical Research: Atmospheres, 126, e2021JD034 888, https://doi.org/10.1029/2021JD034888, 2021.

Lunder, C.: Measurement of Halocarbons and greenhouse gases at Trollhaugen [Dataset], https://doi.org/10.48597/P8CA-KWZG, NILU, Department For Atmospheric Research, EBAS, 2024.

Marks, J. and Bayliss, C.: IAI 2010 anode effect survey results, Aluminium International Today, 23, 15–16,18, https://www.proquest.com/docview/1009072373/abstract/3ECB7B2FFDA6449CPQ/1, 2011.

Miller, B. R., Weiss, R. F., Salameh, P. K., Tanhua, T., Greally, B. R., Mühle, J., and Simmonds, P. G.: Medusa: A Sample Preconcentration and GC/MS Detector System for in Situ Measurements of Atmospheric Trace Halocarbons, Hydrocarbons, and Sulfur Compounds, Analytical Chemistry, 80, 1536–1545, https://doi.org/10.1021/ac702084k, 2008.

MoEFCC: India Fourth Biennial Update Report, Tech. rep., New Delhi, https://unfccc.int/sites/default/files/resource/India%20BUR-4.pdf, 2024.

Mühle, J., Ganesan, A. L., Miller, B. R., Salameh, P. K., Harth, C. M., Greally, B. R., Rigby, M., Porter, L. W., Steele, L. P., Trudinger, C. M., Krummel, P. B., O'Doherty, S., Fraser, P. J., Simmonds, P. G., Prinn, R. G., and Weiss, R. F.: Perfluorocarbons in the global atmosphere: tetrafluoromethane, hexafluoroethane, and octafluoropropane, Atmospheric Chemistry and Physics, 10, 5145–5164, https://doi.org/10.5194/acp-10-5145-2010, 2010.

Pisso, I., Sollum, E., Grythe, H., Kristiansen, N. I., Cassiani, M., Eckhardt, S., Arnold, D., Morton, D., Thompson, R. L., Groot Zwaaftink, C. D., Evangeliou, N., Sodemann, H., Haimberger, L., Henne, S., Brunner, D., Burkhart, J. F., Fouilloux, A., Brioude, J., Philipp, A., Seibert, P., and Stohl, A.: The Lagrangian particle dispersion model FLEXPART version 10.4, Geoscientific Model Development, 12, 4955–4997, https://doi.org/10.5194/gmd-12-4955-2019, 2019.

Prinn, R., Weiss, R., Arduini, J., Choi, H., Engel, A., Fraser, P., Ganesan, A., Harth, C., Hermansen, O., Kim, J., Krummel, P., Lo, Z., Lunder, C., Maione, M., Manning, A., Mitrevski, B., Mühle, J., O'Doherty, S., Park, S., Pitt, J., Reimann, S., Rigby, M., Saito, T., Salameh, P., Schmidt, R., Simmonds, P., Stanley, K., Stavert, A., Steel, P., Vollmer, M., Wagenhäuser, T., Wang, H., Wenger, A., Western, L., Yao, B., Young, D., Zhou, L., and Zhu, L.: The dataset of in-situ measurements of chemically and radiatively important atmospheric gases from the Advanced Global Atmospheric Gas Experiment (AGAGE) and affiliated stations (Version 20250123) [Dataset], https://doi.org/10.60718/0FXA-QF43, NASA Langley Research Center (LaRC) Data Host Facility (DHF), 2025.

Prinn, R. G., Weiss, R. F., Arduini, J., Arnold, T., DeWitt, H. L., Fraser, P. J., Ganesan, A. L., Gasore, J., Harth, C. M., Hermansen, O., Kim, J., Krummel, P. B., Li, S., Loh, Z. M., Lunder, C. R., Maione, M., Manning, A. J., Miller, B. R., Mitrevski, B., Mühle, J., O'Doherty, S., Park, S., Reimann, S., Rigby, M., Saito, T., Salameh, P. K., Schmidt, R., Simmonds, P. G., Steele, L. P., Vollmer, M. K., Wang, R. H., Yao, B., Yokouchi, Y., Young, D., and Zhou, L.: History of chemically and radiatively important atmospheric gases from the Advanced Global Atmospheric Gases Experiment (AGAGE), Earth System Science Data, 10, 985–1018, https://doi.org/10.5194/essd-10-985-2018, 2018.

Ravishankara, A. R., Solomon, S., Turnipseed, A. A., and Warren, R. F.: Atmospheric Lifetimes of Long-Lived Halogenated Species, Science, 259, 194–199, https://doi.org/10.1126/science.259.5092.194, 1993.

Rigby, M., Prinn, R. G., O'Doherty, S., Miller, B. R., Ivy, D., Mühle, J., Harth, C. M., Salameh, P. K., Arnold, T., Weiss, R. F., Krummel, P. B., Steele, L. P., Fraser, P. J., Young, D., and Simmonds, P. G.: Recent and future trends in synthetic greenhouse gas radiative forcing, Geophysical Research Letters, 41, 2623–2630, https://doi.org/10.1002/2013GL059099, 2014.

Say, D., Manning, A. J., Western, L. M., Young, D., Wisher, A., Rigby, M., Reimann, S., Vollmer, M. K., Maione, M., Arduini, J., Krummel, P. B., Mühle, J., Harth, C. M., Evans, B., Weiss, R. F., Prinn, R. G., and O'Doherty, S.: Global trends and European emissions of

https://doi.org/10.5194/egusphere-2025-5656
Preprint. Discussion started: 18 December 2025

tetrafluoromethane (CF_4), hexafluoroethane (C_2F_6) and octafluoropropane (C_3F_8), Atmospheric Chemistry and Physics, 21, 2149–2164, https://doi.org/10.5194/acp-21-2149-2021, 2021.

Stohl, A., Hittenberger, M., and Wotawa, G.: Validation of the lagrangian particle dispersion model FLEXPART against large-scale tracer experiment data, Atmospheric Environment, 32, 4245–4264, https://doi.org/10.1016/S1352-2310(98)00184-8, 1998.

Tabereaux, A. T. and Peterson, R. D.: Chapter 2.5 - Aluminum Production, in: Treatise on Process Metallurgy, edited by Seetharaman, S., pp. 839–917, Elsevier, Boston, https://doi.org/10.1016/B978-0-08-096988-6.00023-7, 2014.

Tan, C., Yu, X., Li, D., Lei, T., Hao, Q., and Guan, D.: Different technology packages for aluminium smelters worldwide to deliver the 1.5 °C target, Nature Climate Change, 15, 51–58, https://doi.org/10.1038/s41558-024-02193-x, 2025.

Tarantola, A.: Inverse Problem Theory and Methods for Model Parameter Estimation, Society for Industrial and Applied Mathematics, http://epubs.siam.org/doi/book/10.1137/1.9780898717921, 2005.

Thacker, W. C.: Data assimilation with inequality constraints, Ocean Modelling, 16, 264–276, https://doi.org/10.1016/j.ocemod.2006.11.001, 2007.

Thompson, R. L. and Stohl, A.: FLEXINVERT: an atmospheric Bayesian inversion framework for determining surface fluxes of trace species using an optimized grid, Geoscientific Model Development, 7, 2223–2242, https://doi.org/10.5194/gmd-7-2223-2014, 2014.

Trudinger, C. M., Fraser, P. J., Etheridge, D. M., Sturges, W. T., Vollmer, M. K., Rigby, M., Martinerie, P., Mühle, J., Worton, D. R., Krummel, P. B., Steele, L. P., Miller, B. R., Laube, J., Mani, F. S., Rayner, P. J., Harth, C. M., Witrant, E., Blunier, T., Schwander, J., O'Doherty, S., and Battle, M.: Atmospheric abundance and global emissions of perfluorocarbons CF_4, C_2F_6 and C_3F_8 since 1800 inferred from ice core, firn, air archive and in situ measurements, Atmospheric Chemistry and Physics, 16, 11 733–11 754, https://doi.org/10.5194/acp-16-11733-2016, 2016.

UNFCCC: Kyoto Protocol to the United Nations Framework Convention on Climate Change, Tech. rep., Kyoto, https://unfccc.int/kyoto_protocol, 1997.

UNFCCC: The Paris Agreement, Tech. rep., Paris, https://unfccc.int/process-and-meetings/the-paris-agreement, 2015.

UNFCCC: Greenhouse Gas Inventory Data - Flexible queries Non Annex I countries, https://di.unfccc.int/flex_non_annex1, 2024a.

UNFCCC: Greenhouse Gas Inventory Data - Flexible queries Annex I countries, https://di.unfccc.int/flex_annex1, 2024b.

Vimont, I., Montzka, S., Andrews, A., Baier, B., Crotwell, M., Hall, B., Handley, P., Higgs, J., Kofler, J., Legard, T., McKain, K., Miller, J., Moglia, E., Mund, J., Neff, D., Newberger, T., Petron, G., Sweeney, C., Turnbull, J., Wolter, S., and NOAA Global Monitoring Laboratory: Atmospheric Dry Air Mole Fractions of CF4 from the NOAA GML Surface and Aircraft Vertical Profile Network. [Dataset], https://doi.org/10.15138/1SDS-1672, NOAA GML, 2025.

Vogel, H. and Friedrich, B.: An Estimation of PFC Emission by Rare Earth Electrolysis, in: Light Metals 2018, pp. 1507–1517, Springer International Publishing, Cham, https://doi.org/10.1007/978-3-319-72284-9_197, 2018.

Vojta, M., Plach, A., Thompson, R. L., and Stohl, A.: A comprehensive evaluation of the use of Lagrangian particle dispersion models for inverse modeling of greenhouse gas emissions, Geoscientific Model Development, 15, 8295–8323, https://doi.org/10.5194/gmd-15-8295-2022, 2022.

Western, L. M., Rigby, M., Mühle, J., Krummel, P. B., Lunder, C. R., O'Doherty, S., Reimann, S., Vollmer, M. K., Adam, B., Fraser, P. J., Ganesan, A. L., Harth, C. M., Hermansen, O., Kim, J., Langenfelds, R. L., Loh, Z. M., Mitrevski, B., Pitt, J. R., Salameh, P. K., Schmidt, R., Stanley, K., Stavert, A. R., Wang, H.-J. R., Young, D., Weiss, R. F., and Prinn, R. G.: Global Emissions and Abundances of Chemically and Radiatively Important Trace Gases from the AGAGE Network, https://doi.org/10.5281/zenodo.15586140, 2025a.

https://doi.org/10.5194/egusphere-2025-5656
Preprint. Discussion started: 18 December 2025

Western, L. M., Rigby, M., Mühle, J., Krummel, P. B., Lunder, C. R., O'Doherty, S., Reimann, S., Vollmer, M. K., Young, D., Adam, B., Fraser, P. J., Ganesan, A. L., Harth, C. M., Hermansen, O., Kim, J., Langenfelds, R. L., Loh, Z. M., Mitrevski, B., Pitt, J. R., Salameh, P. K., Schmidt, R., Stanley, K., Stavert, A. R., Wang, H.-J., Weiss, R. F., and Prinn, R. G.: Global Emissions and Abundances of Chemically and Radiatively Important Trace Gases from the AGAGE Network, Earth System Science Data Discussions, pp. 1–41, https://doi.org/10.5194/essd-2025-348, 2025b.

Wikipedia: List of semiconductor fabrication plants, https://en.wikipedia.org/w/index.php?title=List_of_semiconductor_fabrication_plants&oldid=1313375740, page Version ID: 1313375740, 2025a.

Wikipedia: List of aluminium smelters, https://en.wikipedia.org/w/index.php?title=List_of_aluminium_smelters&oldid=1306018821, page Version ID: 1306018821, 2025b.

Wong, D. S., Fraser, P., Lavoie, P., and Kim, J.: PFC Emissions from Detected Versus Nondetected Anode Effects in the Aluminum Industry, JOM, 67, 342–353, https://doi.org/10.1007/s11837-014-1265-8, 2015.

WSC: Joint Statement of the 15th Meeting of the World Semiconductor Council (WSC), Tech. rep., Fukuoka, Japan, http://www.semiconductorcouncil.org/wp-content/uploads/2016/07/WSC_2011_Joint_Statement.pdf, 2011.

WSC: Joint Statement of the 28th Meeting of the World Semiconductor Council (WSC), Tech. rep., Miyazaki, Japan, http://www.semiconductorcouncil.org/wp-content/uploads/2024/06/2024-WSC-Joint-Statement-FINAL.pdf, 2024.